Heliyon

ELSEVIER

Received:
15 September 2015
Revised:
20 November 2015
Accepted:
12 February 2016

Heliyon 2 (2016) e00079

Quantification of layered patterns with structural anisotropy: a comparison of biological and geological systems

I. Smolyar [a,*], **T. Bromage** [b], **M. Wikelski** [c]

[a] *National Center for Environmental Information/NOAA, 151 Patton Avenue, Asheville, NC 28801, USA*

[b] *Departments of Biomaterials & Biomimetics and Basic Science & Craniofacial Biology, College of Dentistry, New York University, NY 10003 USA*

[c] *Max Planck Institute for Ornithology, Eberhard-Gwinner-Str, Seewiesen, Starnberg 82319, Germany*

* Corresponding author.

E-mail address: igorsmolyar8755@gmail.com (I. Smolyar).

Abstract

Large-scale patterns evident from satellite images of aeolian landforms on Earth and other planets; those of intermediate scale in marine and terrestrial sand ripples and sediment profiles; and small-scale patterns such as lamellae in the bones of vertebrates and annuli in fish scales are each represented by layers of different thicknesses and lengths. Layered patterns are important because they form a record of the state of internal and external factors that regulate pattern formation in these geological and biological systems. It is therefore potentially possible to recognize trends, periodicities, and events in the history of the formation of these systems among the incremental sequences. Though the structures and sizes of these 2-D patterns are typically scale-free, they are also characteristically anisotropic; that is, the number of layers and their absolute thicknesses vary significantly during formation. The aim of the present work is to quantify the structure of layered patterns and to reveal similarities and differences in the processing and interpretation of layered landforms and biological systems. To reach this goal we used N-partite graph

http://dx.doi.org/10.1016/j.heliyon.2016.e00079

and Boolean functions to quantify the structure of layers and plot charts for "layer thickness vs. layer number" and "layer area vs. layer number". These charts serve as a source of information about events in the history of formation of layered systems. The concept of synchronization of layer formation across a 2-D plane is introduced to develop the procedure for plotting "layer thickness vs. layer number" and "layer area vs. layer number", which takes into account the structural anisotropy of layered patterns and increase signal-to-noise ratio in charts. Examples include landforms on Mars and Earth and incremental layers in human and iguana bones.

Keywords: Image processing, Biological morphology, Remote sensing, Aeolian landscapes

1. Introduction

Layered patterns of different sizes and origins are broadly distributed in nature. High-resolution satellite images of large-scale aeolian features on Earth and other planetary surfaces (Ewing et al., 2010; Le Gall et al., 2012; Fitzsimmons, 2007; Rubin, 2006; Rubin et al., 2008; Bourke et al., 2008), Transverse Aeolian Ridges (Wilson and Zimbelman, 2004; Balme et al., 2008; Zimbelman, 2010), and Periodic Bedrock Ridges (Montgomery et al., 2012) consist of numerous layers. Despite differences in size and physical characteristics, there are striking similarities between the configuration of layered terrestrial and extraterrestrial landscapes and of the growth layers of various biological systems such as bone lamellae, fish scales, and tree rings. Typically, layers have numerous breaks and confluences (i.e., bifurcations and merges, Blumberg, 2006), and thus the number and thickness of these layers is a function of the direction of measurement; layered patterns are anisotropic in both size (including thickness and area) and structure. Fig. 1 depicts examples of geological and biological patterns, demonstrating the anisotropy of layered patterns.

Layers form a record of the state of internal and external factors that control the formation of geological (Fishbaugh et al., 2010; Thomas et al., 2005; Bourke et al., 2010; Fenton and Hayward, 2010; Tsoar, 2005) and biological (Casselman, 1983; Klevezal, 1996; Bromage et al., 2009) systems. It is therefore potentially possible to evaluate the structure of layered patterns and recognize events in the history of their formation.

The major problem encountered in the two-dimensional (2-D) analysis of layered patterns is that the structures and sizes of these patterns are characteristically anisotropic. One of the problems inherent in processing layered patterns is that many elements of the procedure for quantifying large-scale anisotropic layered patterns are not formalized and consequently not automated.

http://dx.doi.org/10.1016/j.heliyon.2016.e00079

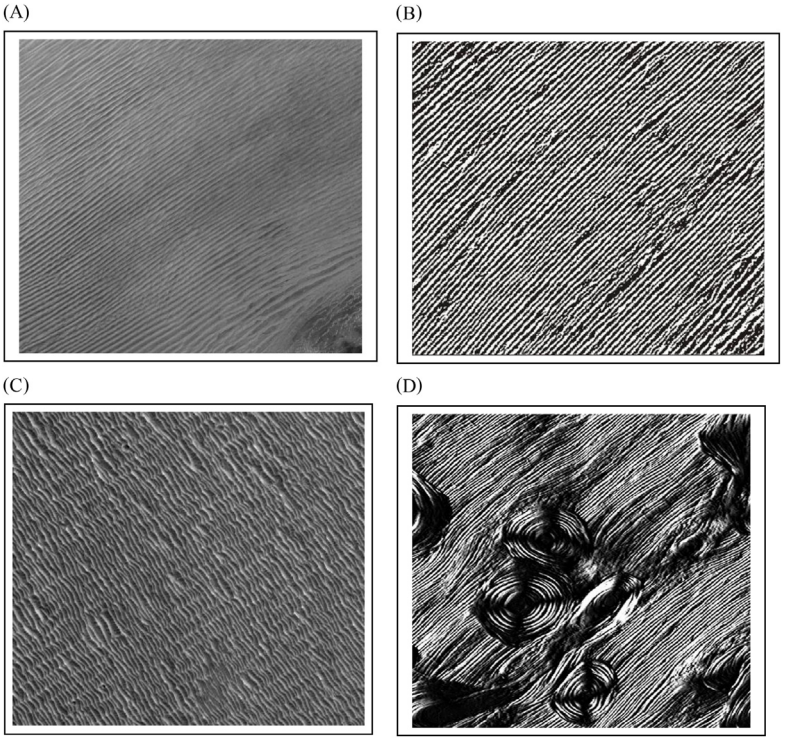

Fig. 1. Samples of biological and geological layered patterns. Biological and geological samples are described in terms of microns and kilometers, respectively. (A) Dunes of Rub' al Khali desert. (B) Cross section of an iguana bone. (C) Layered landform on Mars (ESP_021737_1710_RED). (D) Cross-section of human bone.

The high level of anisotropy is very challenging for mathematicians and computer specialists to formalize.

The empirical M model of anisotropic 2-D layered biological structures was developed to quantify the variability of layer thickness across a 2-D plane (Smolyar and Bromage, 2004). This model is based on a quantitative description of the structure and thickness of layers in N different directions (across a 2-D plane or, more precisely, across N transects); that is, M = {Layer structure, Layer thicknesses in N directions}. Two mathematical tools, the N-partite graph G(N) (Fig. 2A) and Boolean functions (Fig. 2B, C and D), are used to quantify the structure of 2-D layered patterns. Boolean functions and G(N) represent the empirical model of anisotropic 2-D layered structures and, for incremental structures, have been used to construct a time series for "layer thickness vs. layer number (i.e., time)" describing variability of growth rate in fish scales (Smolyar and Bromage, 2004) and human bone lamellae (Bromage et al., 2009; Bromage et al., 2011) across a 2-D plane. The capability of M was extended by developing a fully automated procedure for converting binary images of 2-D layered patterns into N-partite graphs G(N) and Boolean functions, reducing

http://dx.doi.org/10.1016/j.heliyon.2016.e00079

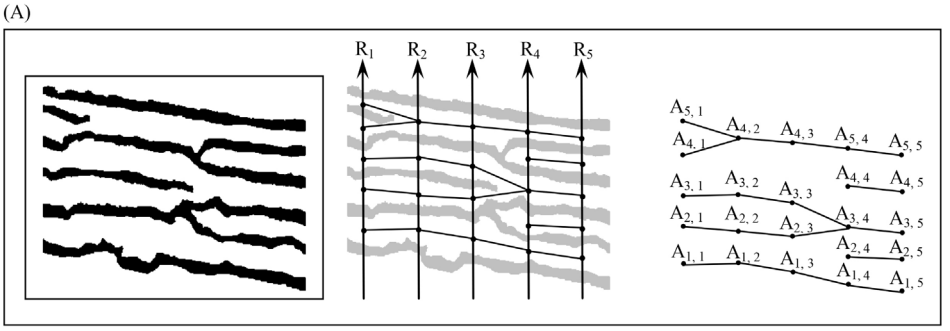

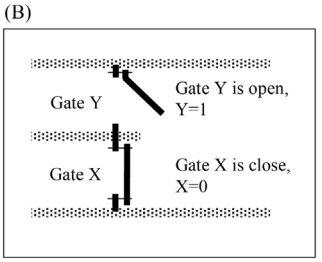

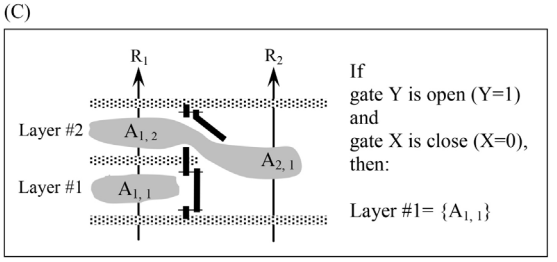

(D)

State of gates		Structure of layers		
X	**Y**	**Layer #1**	**Layer #2**	**Layer #3**
0	0	$A_{1,1}$	$A_{2,1}$	$A_{1,2}$
0	1	$A_{1,1}$	$A_{1,2}$, $A_{2,1}$	-
1	0	$A_{1,1}$, $A_{2,1}$	$A_{1,2}$	-
1	1	This state of doors violated properties of layers		

Fig. 2. Quantifying the anisotropic structure of a layered pattern. More details can be found in Smolyar and Bromage (2004) and Smolyar (2014). (A) Transition of 2-D layered pattern to N-partite graph. (B) Illustration of the concept of "gate open" and "gate closed". The concept allows us to describe the anisotropic structure of a 2-D layered pattern in terms of a Boolean function. (C) Layer structure is a function of the state of gates. (D) Truth Table for the pattern segment depicted in Fig. 2C.

noise in the charts for "layer thickness vs. layer number" and "layer area vs. layer number" and estimating the robustness of variability of layer size across the 2-D plane (Smolyar, 2014). The proposed method is especially relevant given the reproducible nature of the analysis and the huge number of available biological images (Nature Methods, 2012) and satellite images of terrestrial and extraterrestrial surfaces (McEwen et al., 2007; Balme et al., 2008) currently in need of analysis.

The present work quantifies the structure of layered patterns and reveals similarities and differences in the processing and interpretation of layered geological and biological systems. To reach this goal we used N-partite graph and Boolean functions to quantify the structure of layers and plot charts for "layer thickness vs. layer number" and "layer area vs. layer number" for biological and geological systems. These charts describe a fundamental characteristic of living systems (i.e., growth-rate variability of layered pattern

http://dx.doi.org/10.1016/j.heliyon.2016.e00079

across a 2-D plane) since the thickness of a layer is the measure of growth rate at an instance in time. Growth-rate variability in layered patterns is broadly used to identify events in the life history of biological objects (Klevezal, 1996; Casselman, 1983; Bromage et al., 2011).

Two characteristics of thickness of geological layers make it worthwhile to plot charts for "layer thickness vs. layer number" and "layer area vs. layer number" for geological systems and compare them to layered biological systems. First, the thickness of a geological layer (wavelength) is the principal morphometric parameter of a layered landform (Balme et al., 2008). Second, "larger wavelengths probably reflect longer development times and stronger winds" (Yizhaq et al., 2009). Thus, charts for "layer thickness vs. layer number" and "layer area vs. layer number" serve as a source of information about the formation history of layered geological systems. The concept of synchronization of layer formation across a 2-D plane is introduced to develop the procedure for plotting "layer thickness vs. layer number" and "layer area vs. layer number," which takes into account the structural anisotropy of layered patterns.

Notwithstanding the fact that biological and geological layered patterns have structural similarities, there are differences between the processing and interpretation of their images. To the best of our knowledge, these differences have never been investigated. To address this we describe in detail two interrelated concepts: a) layer structure across 2-D patterns, and b) the synchronization of layer formation across a 2-D plane. These concepts form the basis for the quantification of anisotropic structures of layered patterns and describe the similarity and differences in processing and interpreting these systems. Layered patterns of human and iguana bone lamella, the Transverse Aeolian Ridges on Mars, and the dunes of the Rub' al Khali desert on the Arabian Peninsula are used to compare results of the parameterization and interpretation of biological and geological layered systems.

2. Methods

The main focus of the present work is quantifying the anisotropic structure of layered patterns. We used trivial procedures for converting an initial grayscale image into binary mode to calculate the thickness of layers because they are simple but sufficient to justify the applicability of the model.

This section presents a system for processing images of 2-D layered patterns (Smolyar, 2014). The input is a 2-D grayscale layered image in raster format and the output is a set of characteristics of layered patterns that includes:

- Chart A: "layer thickness vs. layer number," which describes the variability of layer thickness across N transects. Chart A is denoted by TH = f(Ln), where TH indicates layer thickness and Ln indicates layer number;

http://dx.doi.org/10.1016/j.heliyon.2016.e00079

- Chart B: "layer area vs. layer number," which describes the variability of layer areas across N transects. Chart B is denoted by AR = f(Ln), where AR indicates area of layers;
- Index of confidence for Charts A and B;
- Signal-to-noise ratio for Charts A and B.

Sections 2.1 and 2.2 outline the method for constructing charts A and B. Focus is given to the idea of layered structures across a 2-D plane by comparing isotropic and anisotropic 2-D layered patterns and noise reduction in charts A and B. Section 2.3 describes the sequence of steps for converting a grayscale image of the 2-D layered landscape into an N-partite graph G(N) and into tables comprising the size of the layers.

2.1. Isotropic structure of 2-D layered patterns

Fig. 3A depicts a layered pattern with isotropic structure; that is, there are no breaks or confluences in the geometrical configuration of layers. The algorithm for plotting charts TH = f(Ln) and AR = f(Ln) is straightforward and consists of the following steps:

1. Plot N parallel transects crossing all layers (Fig. 3B).
2. Label the layers sequentially along transects $R_1, \ldots, R_4$ (Fig. 3C).
3. Describe the structure of the layered pattern using a 4-partite graph (Fig. 3C). In terms of graph theory, the structure of layer $\mathbf{P}_2$ is its path in the 4-partite graph, which is as follows: $\mathbf{P}_2 = (A_{2,1}, A_{2,2}, A_{2,3}, A_{2,4})$ (Fig. 3C).
4. Calculate the thickness of layers along transects $R_1, \ldots, R_4$ (Fig. 3D) and the area of layers between adjacent transects R_1 and R_2, R_2 and R_3, and R_3 and R_4. Average the thickness and area of layers across N transects.
5. Plot charts TH = f(Ln) (Fig. 3E) and AR = f(Ln).

Let $LP(\mathbf{P}_i)$ denote the length of layer $\mathbf{P}_i$ such that $LP(\mathbf{P}_i)$ is equal to the number of vertices crossed by path $\mathbf{P}_i$. In terms of graph theory, $LP(\mathbf{P}_i)$ is the length of path $\mathbf{P}_i$ in G(N) and equal to the number of vertices in $\mathbf{P}_i$. Layers in 2-D patterns with isotropic structure have a one-to-one correspondence between layers situated along transects R_j and R_{j+1}. It follows that:

a. Each layer is crossed by all transects (Fig. 3B); that is, all layers have identical lengths; $LP(\mathbf{P}_1) = LP(\mathbf{P}_2) = LP(\mathbf{P}_3) = LP(\mathbf{P}_4) = 4$ (Fig. 3B);
b. Layers form a totally ordered set, meaning that on a 2-D plane, layer $\mathbf{P}_{i+1}$ is always arranged after $\mathbf{P}_i$ in the direction of labeling (Fig. 3C);
c. Each layer has only one possible path (Fig. 3B and 3C).

http://dx.doi.org/10.1016/j.heliyon.2016.e00079

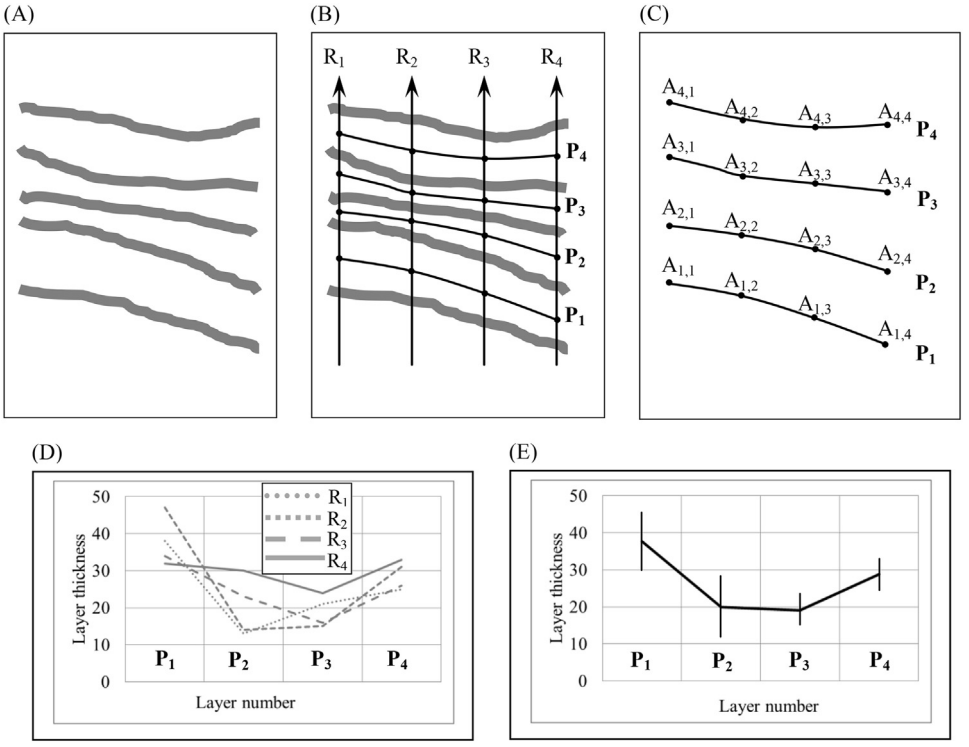

Fig. 3. Variability of layer thickness across a 2-D pattern with isotropic layer structure and anisotropic layer thickness. (A) Sample of the layered pattern. (B) Construction of 4-partite graph G(4). (C) The isotropic structure of G(4) makes it possible to plot only one version of layer structure $\mathbf{P}_1$, $\mathbf{P}_2$, $\mathbf{P}_3$, $\mathbf{P}_4$. (D) Variability of layer thickness along transects R_1, R_2, R_3, R_4. Transect R_j generates chart TH = f_j(Ln). Charts TH = f_1(Ln), . . . , TH = f_4(Ln) are not identical because of anisotropic layer size. (E) Chart averaged over TH = f_1(Ln), . . . , TH = f_4(Ln). Bars show min-max value of layers $\mathbf{P}_1$, $\mathbf{P}_2$, $\mathbf{P}_3$, $\mathbf{P}_4$.

The next section considers the evolution of layer features a), b), and c) and the procedure for plotting charts TH = f(Ln) and AR = f(Ln) for patterns with an anisotropic layer structure.

2.2. Anisotropic structure of 2-D layered patterns

2.2.1. Features of 2-D patterns

Let us change the geometrical configuration of the layered pattern (Fig. 3A) slightly in order to convert it to a 2-D pattern with structural anisotropy (Fig. 4A). For patterns with anisotropic structure, there is obviously no one-to-one correspondence between layers situated along nearby transects (Fig. 4B). For instance, vertex $A_{3,2}$ corresponds to $A_{2,3}$ and $A_{3,3}$ (Fig. 4C). It follows that 2-D layered patterns with structural anisotropy have the following features:

http://dx.doi.org/10.1016/j.heliyon.2016.e00079

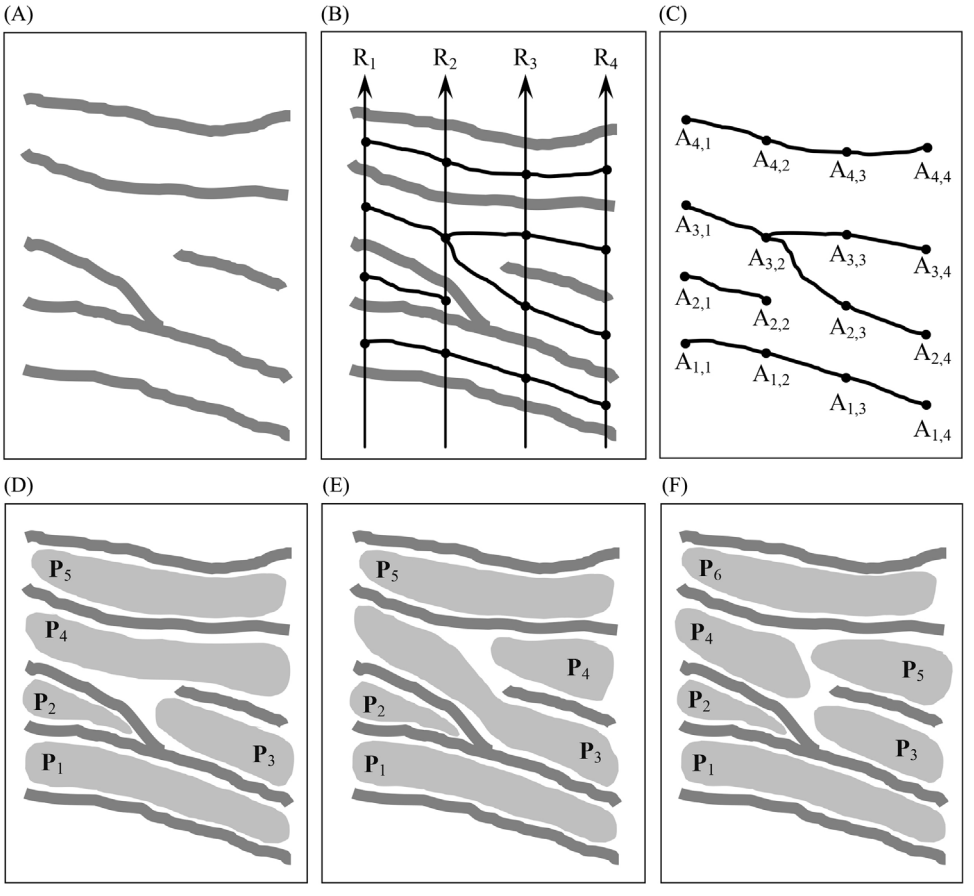

Fig. 4. Steps of the transition from 2-D layer pattern with structural anisotropy into N-partite graph G(N) and samples of different versions of the structure of layers. (A) Sample of breaking and confluence in layer structure (i.e., "layers bifurcate and merge" Blumberg, 2006). (B) Step #1: Draw 4 transects. Arrows on transects show the direction of labeling. Dots represent points of intersection of layers with transects. Two points on two nearby transects are connected by an edge if they belong to the same layer. (C) Step #2: Labeling of points of intersections of transects with layers, resulting in 4-partite graph G(4). (D) Version #1 of the structure of layers. (E) Version #2 of the structure of layers. (F) Version #3 of the structure of layers.

a) Some layers are crossed by fewer than N transects. For instance, layer $\mathbf{P}_2$ (Fig. 4D) and layer $\mathbf{P}_4$ (Fig. 4 E) are each crossed by two transects;

b) Layers form a partially ordered set (Anderson, 2001; p. 87), meaning that for at least two layers it is impossible to define the ordering relation. For instance, layers $\mathbf{P}_4 = (A_{3,1}, A_{3,2})$ and $\mathbf{P}_5 = (A_{3,3}, A_{3,4})$ are not related (Fig. 4F);

c) Some layers have more than one possible path. For instance, layer $\mathbf{P}_4$ has three different versions of paths, presented respectively in Fig. 4D, E, and F.

http://dx.doi.org/10.1016/j.heliyon.2016.e00079

The general scheme for constructing TH = f(Ln) and AR = f(Ln) for a 2-D layered pattern with anisotropic structure is the same as for patterns with isotropic structure: draw the transects, measure the size of layers, develop an N-partite graph G(N) and use it to describe the structure of layers, and average the size of layers across transects $R_1, \ldots, R_N$, resulting in charts TH = f(Ln) and AR = f(Ln). However, the procedures for quantifying layer structure and averaging across N transects are different because features a)–c) of 2-D layered patterns with structural anisotropy are opposite to the corresponding features of patterns with structural isotropy.

2.2.2. *Quantifying layer structure across a 2-D plane*

In terms of graph theory, the problem of quantifying layer structure in a 2-D plane can be described as a problem of finding paths in G(N) that include all vertices $A_{i,j}$ (Roberts, 1976). By analogy with biological layered patterns (Smolyar and Bromage, 2004):

Paths in graph G(N) cannot intersect, merge, or cross transect R_j more than once (1)

For instance, three versions of layer structure depicted in Fig. 4D, E, and F satisfy condition Eq. (1).

The problem of quantifying layered structures is that in order to plot charts TH = f(Ln) and AR = f(Ln), it is necessary to find among many different versions of layer structure one "best" version, or to plot and analyze many different versions and to take the average. The idea of a "best" path applicable to different categories of layered systems is difficult or even impossible to formalize. Thus, instead of constructing one "best" version of paths, possible versions of paths, $V_1, \ldots, V_q, \ldots, V_k$, are plotted. Version V_q is associated with charts $TH = f_q(Ln)$ and $AR = f_q(Ln)$, where q denotes the arbitrarily chosen version of the state of the "gates" in the Boolean functions of a 2-D layered pattern (Fig. 2B). However, due to numerous discontinuities and convergences, a phenomenal number of possible versions may be found in only a small portion of a layered pattern (see landform examples in Fig. 1A and C). One possible solution to this predicament is to select two opposite versions of layer structure, V_q and V_{-q}, where V_{-q} is the version of layer structure with a state of "gates" opposite to V_q. The two opposite versions—V_q and V_{-q}—allow more confidence when estimating the robustness of $TH = f_q(Ln)$ and $AR = f_q(Ln)$ with regard to the variability of layered structure than would two randomly chosen versions (Smolyar and Bromage, 2004).

Fig. 5 illustrates the basic steps of the procedure for converting a 2-D layered pattern into two opposite versions of layer structure, V_q and V_{-q}. The initial

http://dx.doi.org/10.1016/j.heliyon.2016.e00079

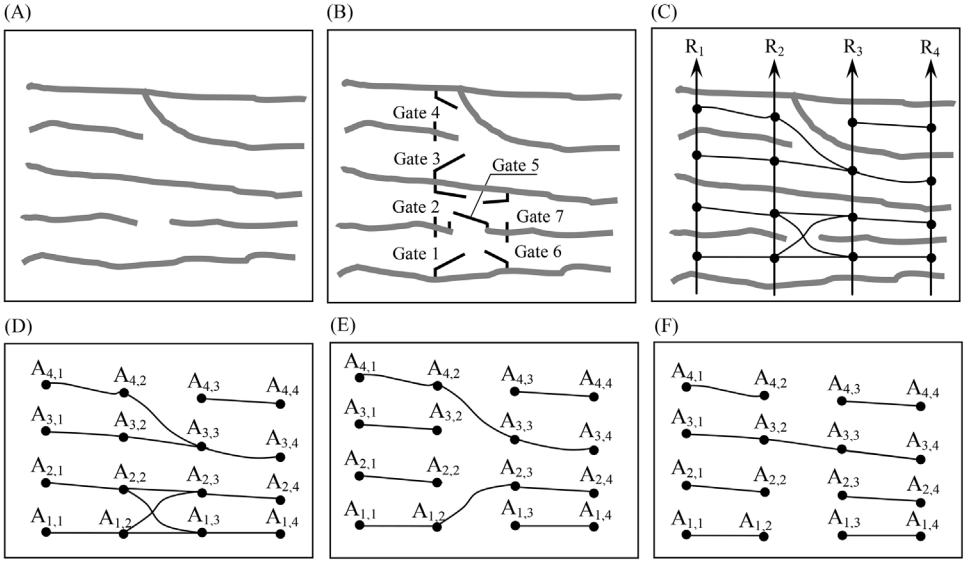

Fig. 5. Constructing different versions of layer structure. (A) Sample of pattern with anisotropic layer size and structure. (B) Transition of layered pattern into Boolean functions: Position of "gates" defines all possible versions of layered structure. The number of all possible versions equals $2^{\text{number of "gates"}} = 2^7 = 128$. (C) Conversion of a layered pattern with anisotropic structure and size into 4-partite graph. (D) Structure of layered pattern presented in the form of a 4-partite graph. (E) Sample of strictly ordered layers. (F) Sample of partially ordered layers.

pattern (Fig. 5A) is presented using Boolean functions consisting of seven "gates" (Fig. 5B). The possible number of different versions of paths is equal to $2^{\text{number of "gates"}} = 2^7 = 128$. Not all of the 128 versions of layer structure satisfy condition (1); these versions therefore cannot be used to construct $TH = f_q(Ln)$ and $AR = f_q(Ln)$. Transforming the sampling area of the layered pattern (Fig. 5C) into G(N) results in a 4-partite graph (Fig. 5D). The state of the seven "gates" is described by binary vector $X = (x_1, \ldots, x_f, \ldots, x_7)$, where $x_f = 1$ means that "gate" x_f is open and $x_f = 0$ means that x_f is closed. Two opposite versions of the state of gates $X_q = (1, 0, 0, 1, 1, 0, 1)$ and $X_{-q} = (0, 1, 1, 0, 0, 1, 0)$ generate two opposite versions of layer structure, V_q (Fig. 5E) and V_{-q} (Fig. 5F). The proposed method is used in Section 3 to quantify the variability of layer size across 2-D layered patterns of landforms and lamella bone.

2.2.3. Averaging layer size across a 2-D plane

Consider *k* versions of layer structure for a 2-D layered landform. For instance, Fig. 4D, E, and F depict three versions of layer structure. Let us plot charts $TH = f_1(Ln)$, $TH = f_2(Ln)$, and $TH = f_3(Ln)$ for each version. The sequence of these charts can be interpreted as three measuring cycles that quantify the variability of layer thickness across a 2-D layered pattern. In other words, we

http://dx.doi.org/10.1016/j.heliyon.2016.e00079

made three independent measurements of pattern features. Averaging charts TH = f_1(Ln), TH = f_2(Ln), and TH = f_3(Ln) allows the signal-to-noise ratio in TH = F(Ln) to be increased proportional to the square root of the number of measurement cycles (van Drongelen, 2007), where TH = F(Ln) is the result of averaging these three charts. Thus, one version q of path structure leads to chart TH = f_q(Ln) with signal-to-noise ratio equal to 1, and chart TH = F(Ln) averaged over *k* charts has a signal-to-noise ratio of $\sqrt{k}$.

2.2.4. Averaging layer structure across a 2-D plane

Consider how averaging charts TH = f_1(Ln) and TH = f_2(Ln) affects the correspondence between sequential layer numbers on the x-axis of the average chart TH = F(Ln) and the corresponding sequential layer numbers on a 2-D layered pattern. Averaging the thickness of two layers with different versions of structure **P**(structure version 1) and **P**(structure version 2) necessitates averaging layer structure. The averaging operation with respect to layer structure implies the union of the structure of two layers:

$$P_{average}\text{ (structure version 1, structure version 2) = P(structure version 1) U P (structure version 2),} \quad (2)$$

where **U** indicates the union of two structures. It follows from Eq. (2) that there is a one-to-one correspondence between a layer on the 2-D pattern and the corresponding layer in chart TH = F(Ln) if averaged layers have identical structure. This statement is also true for a 2-D pattern with structural isotropy.

If **P** (structure version 1) ≠ **P** (structure version 2), then two layers with different structures contribute to the calculation of the average thickness of point p on the x-axis of TH = F(Ln). Thus, there is no one-to-one correspondence between the sequential number of point p on the x-axis of the chart TH = F(Ln) and the corresponding layer on the 2-D pattern. In other words, each point on the x-axis of chart TH = F(Ln) corresponds to several layers of the 2-D pattern. The geometric configuration of these layers is defined by Eq. (2). The opposite statement is also correct: one layer of a 2-D pattern could contribute to calculating the average thickness of different points on the x-axis of TH = F (Ln). Thus, two opposite tendencies exist in the construction of TH = F(Ln) and AR = F(Ln); that is, reducing noise in TH = F(Ln) and AR = F(Ln) is always accompanied by an increase in the uncertainty of setting correspondence between point p on charts TH = f_q(Ln) and AR = f_q(Ln) and corresponding layer $\mathbf{P}_p$ on the 2-D pattern. The compromise between these tendencies depends on the category of a pattern and the goals of its analysis. Section 3 provides an example of setting correspondence between TH = F(Ln) on dunes in the Rub' al Khali desert.

http://dx.doi.org/10.1016/j.heliyon.2016.e00079

2.2.5. Length of layers as a noise measure in TH = F(Ln) and AR = F(Ln)

From features of anisotropic layers it follows that different layer lengths are the source of different levels of assurance that layer sizes represent real pattern features rather than noise (Smolyar and Bromage, 2004). For instance, consider a sampling area consisting of 200 transects spaced one meter apart. It would seem reasonable to assume that layers of average size that cross only several transects are more likely to be noise compared to layers of average size that cross more than 100 transects. Thus, in order to reduce noise in charts TH = f(Ln) and AR = f(Ln), the shortest layers could be ignored. Experiments in reducing noise in charts TH = f(Ln) and AR = f(Ln) by manipulating the length of layers are presented in Section 3.

2.2.6. Index of confidence

The index of confidence, ICnf(TH, AR), is the measure of the number of structural details of the 2-D layered landform used to construct charts TH = f (Ln) and AR = f(Ln) such that ICnf(TH) and ICnf(AR) is the ratio of the sum of the area of all layers, S(all layers), which is used to construct TH = F(Ln) and AR = F(Ln) for the area of the 2-D pattern situated between the first, R_1, and last, R_N, transects $S(R_1, R_N)$:

$$ICnf\ (TH) = ICnf(AR) = S(\text{all layers})/S(R_1, R_N). \quad (3)$$

When ICnf (TH, AR) = 1, charts TH = F(Ln) and AR = F(Ln) represent all structural details of the layered landscape. When ICnf (TH, AR) = 0, only one transect is used to construct TH = f(Ln) and AR = f(Ln), meaning that the 2-D layered pattern with anisotropic structure has been converted to a 1-D pattern, and the notion of "layer area" is therefore not applicable. Confidence index ICnf is useful for estimating the robustness of TH = f(Ln) and AR = f(Ln) with regard to the variability of many of the parameters that TH = f(Ln) and AR = f(Ln) depend upon. For instance, ICnf allows the number of transects needed to construct TH = F(Ln) and AR = F(Ln) to be known for different categories of layered patterns at different spatial resolutions.

2.2.7. Plotting charts TH = F(Ln) and AR = F(Ln)

The procedure for plotting charts TH = F(Ln) and AR = F(Ln) consists of the following steps:

i) Plot charts TH = f_q(Ln) and AR = f_q(Ln) for one version, V_q, of layer structure. The signal-to-noise ratio is equal to 1 for these charts.

http://dx.doi.org/10.1016/j.heliyon.2016.e00079

ii) Plot charts for k versions of the structure of layers and average them, resulting in TH = F(Ln) and AR = F(Ln). The signal-to-noise ratio is equal to $\sqrt{k}$ for these charts.

iii) Calculate the index of confidence for TH = F(Ln) and AR = F(Ln).

iv) Remove layers crossed by only one transect from chart TH = F(Ln) and AR = F(Ln), resulting in TH = F_1(Ln) and AR = F_1(Ln), and calculate the index of confidence for TH = F_1(Ln) and AR = F_1(Ln).

v) Repeat previous step N-1 times, removing sequentially from TH = F(Ln) and AR = F(Ln) layers crossed by 2, 3, . . . , N-1 transects, and calculate the index of confidence for each version of the charts.

vi) If the sequence of charts TH = F_1(Ln), TH = F_2(Ln), . . . , TH = F_i(Ln) has a high index of confidence, then these charts are averaged to give an additional increase in the signal-to-noise ratio for the resulting charts.

Thus, averaging the charts allows us to improve the signal-to-noise ratio in TH = f(Ln) and AR = f(Ln) twice: first by averaging charts for different versions of the structure of layers and second by averaging charts with high levels of the index of confidence.

2.3. Image processing

The aim of the image-processing procedure is to formalize the stages of converting the initial grayscale image of a 2-D layered landform with structural anisotropy into an N-partite graph G(N) and tables comprising the thickness and area of layers across a 2-D plane. The present section describes the general scheme for converting initial layered patterns into graphs G(N) and Boolean functions and plotting charts "layer thickness vs. layer number" and "layer area vs. layer number." The scheme consists of five stages (Smolyar, 2014).

First, an initial grayscale image is converted into a binary image, which is then converted into Comma Separated Values (CSV) format. Second, the image is filtered. Values of black and white thresholds are determined empirically according to image size and resolution. Third, transects R_1, . . . , R_N are drawn quasi-perpendicular to layers, and the thicknesses of layers along the transects are calculated. Fourth, an N-partite graph is constructed and the area of layers situated between adjacent transects R_j and R_{j+1} is calculated. Fifth, versions V_1, . . . , V_q, . . . , V_k of the layered structure are calculated. For each version of V_q, charts TH = f_q(Ln) and AR = f_q(Ln) are plotted as described in Section 2.2. Charts TH = f_1(Ln), . . . , TH = f_q(Ln), . . . , TH = f_k(Ln) are averaged, resulting in chart TH = F(Ln), and AR = f_1(Ln), . . . , AR = f_q(Ln), . . . , AR = f_k(Ln) are averaged, resulting in AR = F(Ln). The signal-to-noise ratio equals 1 for charts TH = f_q(Ln) and AR = f_q(Ln) and $\sqrt{k}$

http://dx.doi.org/10.1016/j.heliyon.2016.e00079

for charts TH = F(Ln) and AR = F(Ln). Finally, indices of confidence are calculated for TH = F(Ln) and AR = F(Ln). Technical details of image processing are presented in Sections 2.3.1 – 2.3.6

2.3.1. Converting grayscale images to black and white

Because the connectivity of vertices in the N-partite graph is described using binary terms (i.e., connected/disconnected), constructing the graph is most convenient if the image of the layered pattern is in black and white. Thus, converting the initial grayscale image to black and white is the starting point for pattern processing.

Grayscale images are constructed from pixels with an array of values from 0 to 255. White pixels have a value of 255, black pixels have a value of 0, and values between 0 and 255 are various shades of gray. Two protocols are considered for converting grayscale images of 2-D layered landforms into black-and-white images.

Protocol #1 is used to process images of layered landforms with relatively simple anisotropy and less than 100 layers. The protocol includes two phases: 1) upsampling the pattern (Huss, 2001, pp. 92–97) and 2) choosing a threshold for converting the image to black and white (Huss, 2001, pp. 30–36). If the value of a pixel is greater than or equal to the threshold, the output will be a white pixel; if the value is less than the threshold, the output will be a black pixel. Fig. 6A depicts the original grayscale image (a fragment of ESP_016036_1370) and Fig. 6B shows the results of image upsampling.

Protocol #2 is used to process images with more complicated structures and more than 100 layers. This protocol is similar to Protocol #1 but includes an additional step: an emboss filter is applied between the upsampling and threshold choice steps to enhance the landform layers of the grayscale image (Huss, 2001, p. 425). Fig. 6C shows the results of processing the image using Protocol #2.

After the final pixel values are determined in either protocol, the value of each pixel is presented in Comma Separated Values (CSV) format, where the XY index of a cell in the electronic Table represents the XY coordinates of the pixel on image of the 2-D plane. Commercially available software such as ArcGIS provides tools for this procedure. The output of either protocol is a black-and-white image converted to a CSV file (Fig. 6D). This file is then used to automate the process of converting images of layered patterns into pure mathematical objects (i.e., N-partite graphs and Boolean functions).

http://dx.doi.org/10.1016/j.heliyon.2016.e00079

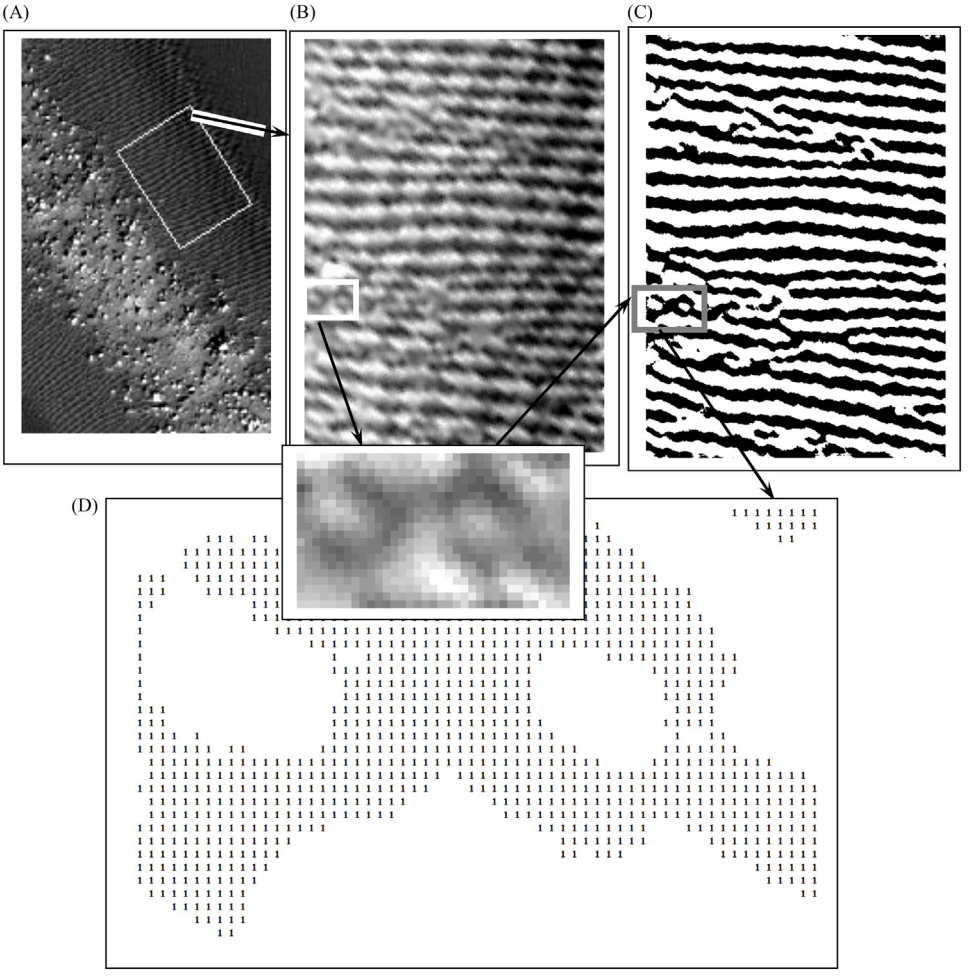

Fig. 6. Converting grayscale images to black and white. (A) Initial image (ESP_016036_1370). (B) Grayscale image before upsample and emboss. (C) Grayscale image after upsample (500%) and emboss. (D) Fragment of the black-and-white image in Comma Separated Values format.

2.3.2. Layer thickness

Layer thickness is an easily measurable parameter that is broadly used for solving various biological and geological problems (Balme et al., 2008; Bromage et al., 2009). Layer thicknesses are measured along transects $R_1, \ldots, R_j, \ldots, R_N$ (Fig. 7A and B). In the present case, transects can be considered as straight lines without any loss of generality, and layers are assumed to be perpendicular to transects. A layer crossed by R_j is described by: (i) layer number, (ii) layer thickness (Fig. 7B and C), and (iii) forming front (Fig. 7B and C). Inputs of the algorithm for calculating layer thickness are the XY coordinates of pixels comprising transects $R_1, \ldots, R_N$ and the black-and-white image of the layered landform in CSV format (Fig. 6D). Black pixels are

http://dx.doi.org/10.1016/j.heliyon.2016.e00079

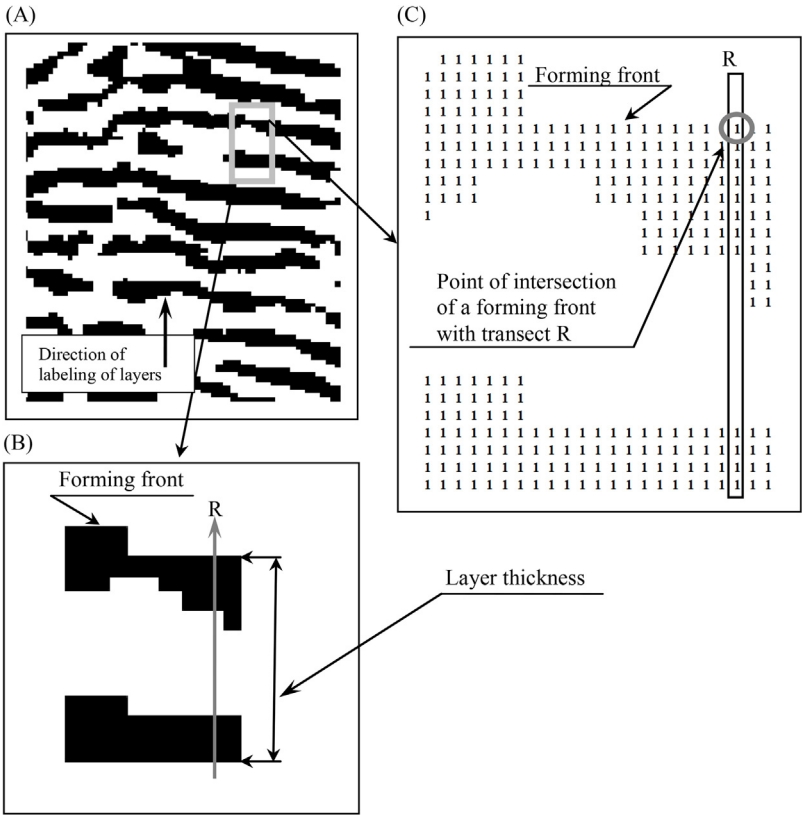

Fig. 7. Principal elements of 2-D layered pattern: a) direction of layer labeling; b) forming front; c) layer thickness; d) point of intersection between forming front and transect R. (A) Initial pattern in raster format illustrating the direction of layer labeling. (B) Fragment of the initial pattern in raster format illustrating layer thickness and forming front. (C) Fragment of the initial pattern in Comma Separate Values format illustrating the forming front and point of intersection between forming front and transect R.

designated as the foreground of the pattern and have a value of 1. White pixels are designated as the background of the pattern and have no value. The algorithm consists of the following steps:

a. Draw transects $R_1, \ldots, R_N$.

b. Calculate the coordinates of the points where layers $\mathbf{P}_1$ and $\mathbf{P}_2$ intersect with transect R_1 (Fig. 7C).

c. Calculate the thickness $w(\mathbf{P}_i)_j$ of layer $\mathbf{P}_i$, which is the distance between two adjacent forming fronts, along transect R_j, (Fig. 7B and C).

d. Repeat steps 1 and 2 for all layers along transects $R_2, \ldots, R_j, \ldots, R_N$, which results in Table T_N containing N columns. Column j of Table T_N comprises the layer thicknesses along transect R_j.

http://dx.doi.org/10.1016/j.heliyon.2016.e00079

2.3.3. Layered pattern segmentation

Filtering the black-and-white image of a layered pattern, constructing the N-partite graph, and calculating the area of layers is accomplished using pattern segmentation and labeling (Rosenfeld and Kak, 1982). In terms of pattern recognition, a forming front is a segment consisting of eight-connected black pixels, also defined as the set of Moore-neighborhood pixels. The size of a segment is the number of eight-connected black pixels of which it is made up.

The procedure for segmenting black-and-white images (Fig. 8A) used here is vastly simpler than the procedure for segmenting color or grayscale images because the connectivity of black pixels can be described in binary terms. The input for the procedure (a black-and-white image in CSV format) is stored digitally in a Table format using a spreadsheet program such as Excel (Fig. 6D). Black pixels are designated as the foreground of the pattern and white pixels are background (Fig. 8B). The segmentation procedure consists of the following steps:

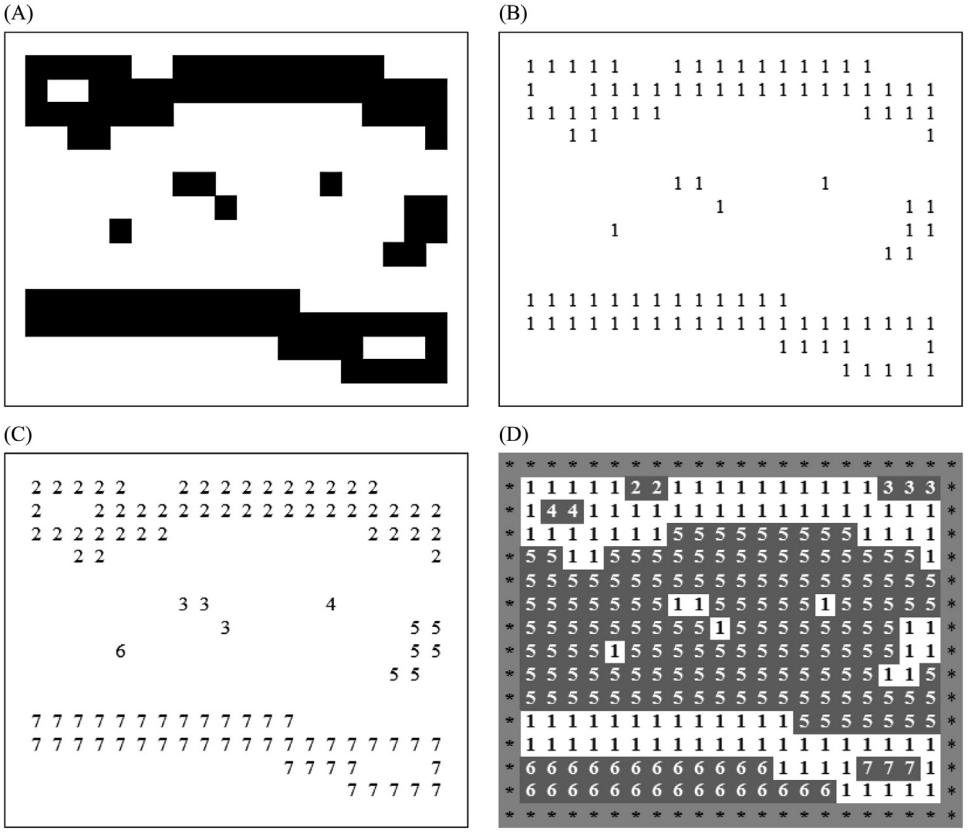

Fig. 8. Segmenting the layered pattern. (A) Black-and-white image in raster format. (B) Black-and-white image in Comma Separate Values format. (C) Segmentation: black pixels are foreground; white pixels are background. (D) Segmentation: black pixels are background; white pixels are foreground.

http://dx.doi.org/10.1016/j.heliyon.2016.e00079

1. The first label ($Label_1$) is assigned an initial value, which is used to label black pixels; therefore $Label_1 = 2$;
2. Scanning the pattern from left to right and then from top to bottom, the first unlabeled black cell is assigned $Label_1$;
3. All black pixels that are 8-connected to the $Label_1$ pixel are also assigned $Label_1$;
4. Steps 2–3 are repeated, until all black pixels have been assigned labels (Fig. 8C);
5. The size of each segment (i.e., the number of pixels making up each segment) is calculated.

The same algorithm can also be used to segment layered patterns in which white pixels have been designated as foreground and black pixels as background (as in Fig. 8D). In order to segment the white pixels, the pattern must first be surrounded by a frame, which allows the algorithm to search for Moore neighborhoods within the frame. The frame (Fig. 8D) is made up of asterisks, which are neither background nor foreground in the image.

2.3.4. Pattern filtering

Filtering a layered pattern removes elements of the pattern that are not associated with layers. There are two types of such elements. The first is black segments with a size (i.e., number of pixels) less than a particular threshold (BlackThreshold), and the second is white holes in black segments with a size less than a particular threshold (WhiteThreshold). The present work chooses values for BlackThreshold and WhiteThreshold empirically. For instance, if the average size of black segments is 100 pixels, then segments of less than five pixels could be eliminated with a high level of confidence. Threshold values should be increased if initial image quality is low.

2.3.5. Constructing the N-partite graph

The inputs for constructing the N-partite graph are two Excel spreadsheets, the first containing a black-and-white image in CSV format (Fig. 9A) and the second containing transects in CSV format. The algorithm for constructing the N-partite graph includes the following steps:

1. Calculate the XY coordinates of pixels comprising transects R_j and R_{j+1};
2. Calculate the XY coordinates of the pixels located at the intersection of transect R_j with white pixels $pw_{1,j}$, $pw_{2,j}$, $pw_{3,j}$, $pw_{4,j}$ immediately adjacent to

http://dx.doi.org/10.1016/j.heliyon.2016.e00079

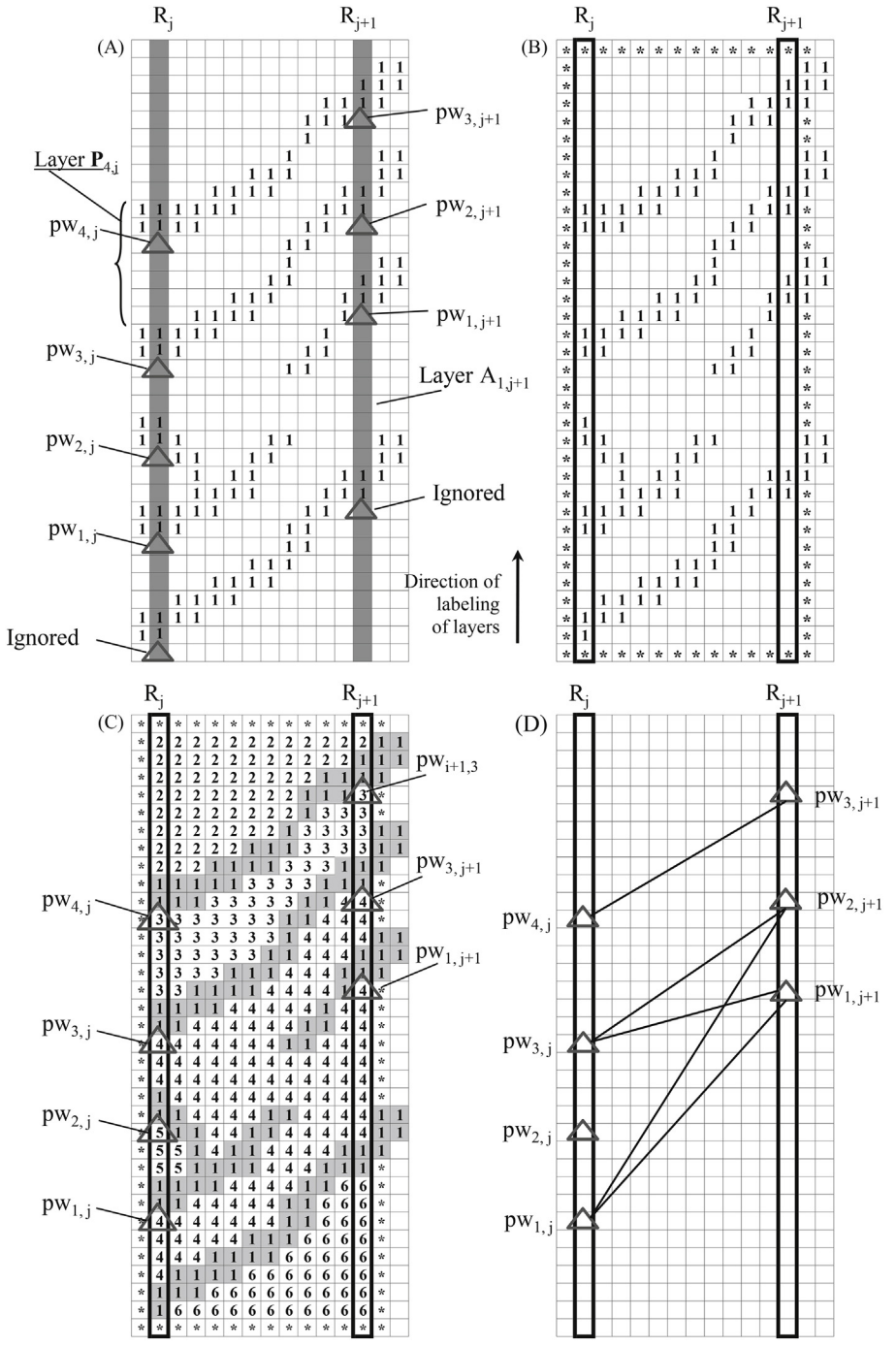

Fig. 9. Converting fragment of 2-D layered pattern situated between two adjacent transects into a bipartite graph. (A) Black-and-white image in Comma Separate Values format situated between two adjacent transects R_j and R_{j+1}. Triangles indicate the position of white pixels immediately adjacent to the forming fronts of layers. Triangles represent the vertex of the bipartite graph. (B) The area between adjacent transects R_j and R_{j+1} is surrounded by a frame asterisks. (C) Segmentation of area of layered pattern between R_j and R_{j+1}: white pixels are foreground. (D) Triangles on opposite transects are connected if they belong to the same segment.

http://dx.doi.org/10.1016/j.heliyon.2016.e00079

the forming fronts of layers $\mathbf{P}_{1,j}$, $\mathbf{P}_{2,j}$, $\mathbf{P}_{3,j}$, $\mathbf{P}_{4,j}$ (Fig. 9A). These white pixels are the vertices of graph G(N) along transect R_j;

3. Calculate the XY coordinates of the pixels located at the intersection of transect R_{j+1} with white pixels $pw_{1,j+1}$, $pw_{2,j+1}$, $pw_{3,j+1}$ immediately adjacent to the forming fronts of layers $\mathbf{P}_{1,j+1}$, $\mathbf{P}_{2,j+1}$, $\mathbf{P}_{3,j+1}$ (Fig. 9A);
4. Draw a rectangular frame of asterisks around the area between adjacent transects R_j and R_{j+1} (Fig. 9B);
5. Apply the algorithm for segmenting and labeling white pixels within the frame (Fig. 9C);
6. Connect vertices (white pixels) that belong to the same segment with a line if they fall on different transects (Fig. 9D);
7. Repeat step (6) for all pixels on R_j. This step creates a bipartite graph describing the structure of the layered landform between adjacent transects R_j and R_{j+1}.
8. Repeat steps (1)–(7) for all pairs of adjacent transects R_2–R_3, R_3–R_4, . . . , R_{N-1}–R_N.

2.3.6. Area of layers

Area $S(\mathbf{P}_{i,j})$ of layer $\mathbf{P}_{i,j}$ comprises the set of black pixels and the set of their immediately adjacent white pixels. Pixel $pb_{i,j}$ (indicated by a circle in Fig. 10A) represents the point of intersection between the black component of layer $\mathbf{P}_{i,j}$ and transect R_j; pixel $pw_{i,j}$ (indicated by a triangle in Fig. 10A) represents the point of intersection between the white component of layer $\mathbf{P}_{i,j}$ and transect R_j. Because the distance between any pair of adjacent transects R_j and R_{j+1} remains constant across the sampling area, it is possible to compare the results of calculating the area of layers between any pair of adjacent transects R_j and R_{j+1}.

The input for calculating the area of layers is an Excel spreadsheet containing a black-and-white image in CSV format (Fig. 10A). The output of the algorithm is a Table containing N-1 columns. Column j contains the areas of layers situated between adjacent transects R_j and R_{j+1}. The algorithm for calculating area $S(\mathbf{P}_{i,j})$ consists of the following steps:

1. Assign sequential numbers to pixels $pb_{i,j}$ and $pw_{i,j}$ (Fig. 10A);
2. Calculate the coordinates of points $pb_{i,j}$ and $pw_{i,j}$, where layer $P_{i,j}$ intersects with transect R_j (Fig. 10A);
3. Draw a rectangular frame of asterisks around the area between adjacent transects R_j and R_{j+1} in order to segment the black and white pixels (Fig. 10B);

http://dx.doi.org/10.1016/j.heliyon.2016.e00079

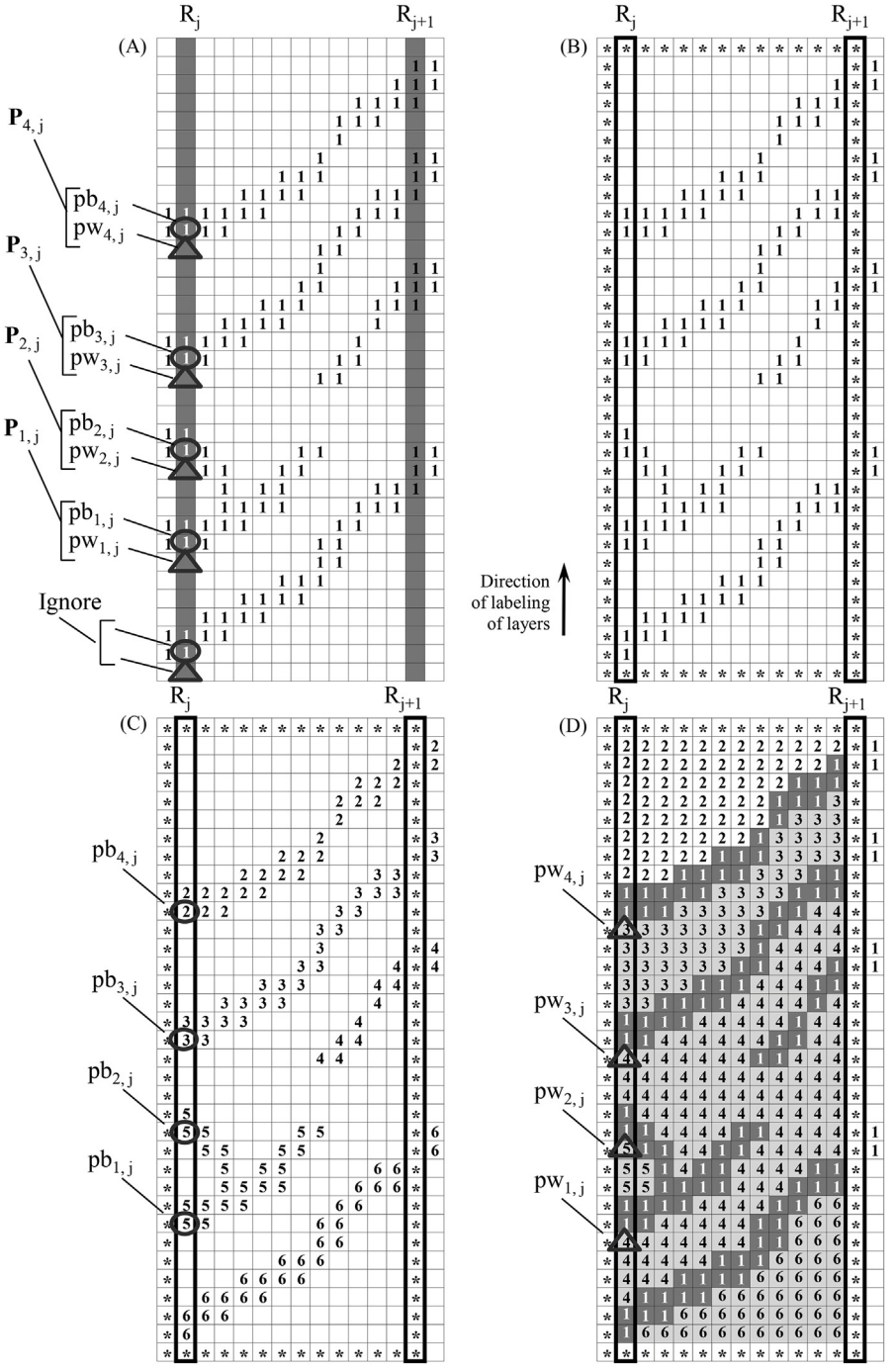

Fig. 10. Procedure for calculating layer area. (A) Circles represent black components of the layer; triangles represent white components. (B) A frame consists of asterisks covering the area between transects R_j and R_{j+1}. The layer area within this frame is to be calculated. (C) Segmentation of black pixels results in area of black components of layers. (D) Segmentation of white pixels results in area of white components of layers.

http://dx.doi.org/10.1016/j.heliyon.2016.e00079

4. Apply the algorithm for fragmenting and labeling (Fig. 10C) to label the forming fronts between transects R_j and R_{j+1}. In this case, the foreground of the layered pattern is designated as pixels with value 1 (black pixels) and the background is pixels with no value (white pixels); the framing asterisks are neither background nor foreground. Fragment number K is assigned to each black pixel $pb_{i,1}$.
5. Calculate the areas of the fragments by counting the number of pixels comprising each fragment. One black fragment could potentially form more than one layer as a result of breaks and confluences in the layers' geometrical structure. If fragment K creates forming fronts for U layers, then the area of forming fronts for the individual layer is equal to the area of fragment K divided by U;
6. Calculate the value of $U(pb_{i,j})$ for each $pb_{i,j}$, where $U(pb_{i,j})$ denotes the number of layers formed by fragment $K(pb_{i,j})$;
7. Calculate area $S(P_{i,j})_{blackpixels}$ of layer $P_{i,j}$:
   - $S(P_{i,j})_{blackpixels} = S[K(pb_{i,j})]/U(pb_{i,j})$.
   - $S[K(pb_{i,j})]$ is the area of fragment K;
8. Repeat steps (1)–(7) for transects R_2–R_3, . . . , R_{N-1}–R_N;
9. Repeat steps (1)–(8) to calculate the area $S(\mathbf{P}_{i,j})_{whitepixels}$ of white component $pw_{i,j}$ of layer $\mathbf{P}_{i,j}$ (Fig. 10D):
   - $S(\mathbf{P}_{i,j})_{whitepixels} = S[K(pw_{i,j})]/U(pw_{i,j})$.
   - Calculate area $S(\mathbf{P}_{i,1})$ of layer $\mathbf{P}_{i,j}$ between transects R_j and R_{j+1}:
   - $S(\mathbf{P}_{i,j}) = S(\mathbf{P}_{i,j})_{blackpixels} + S(\mathbf{P}_{i,j})_{whitepixels}$;
10. Repeat step (9) for transects R_2–R_3, . . . , R_{N-1}–R_N.

3. Results

3.1. Mars landform: noise reduction and index of confidence

Images of Martian landforms such as Transverse Aeolian Ridges (TARs) are an example of 2-D layered landforms with anisotropic structure and size. The "ripple field" in Eastern Candor Chasm in E03-02283 (Wilson and Zimbelman, 2004) is used to test the proposed method. The parameters of the procedure for converting a grayscale pattern (Fig. 11A) to binary (Fig. 11B) are as follows (Section 2.3.1):

- Resample (Huss, 2001, p. 92–97). Width: 500%; height: 500%.
- Emboss (Huss, 2001, p. 425). Depth: 20; level: 495; direction: 22.
- Convert image to binary (Huss, 2001, p. 30–36). Conversion method: line art; threshold: 65.

http://dx.doi.org/10.1016/j.heliyon.2016.e00079

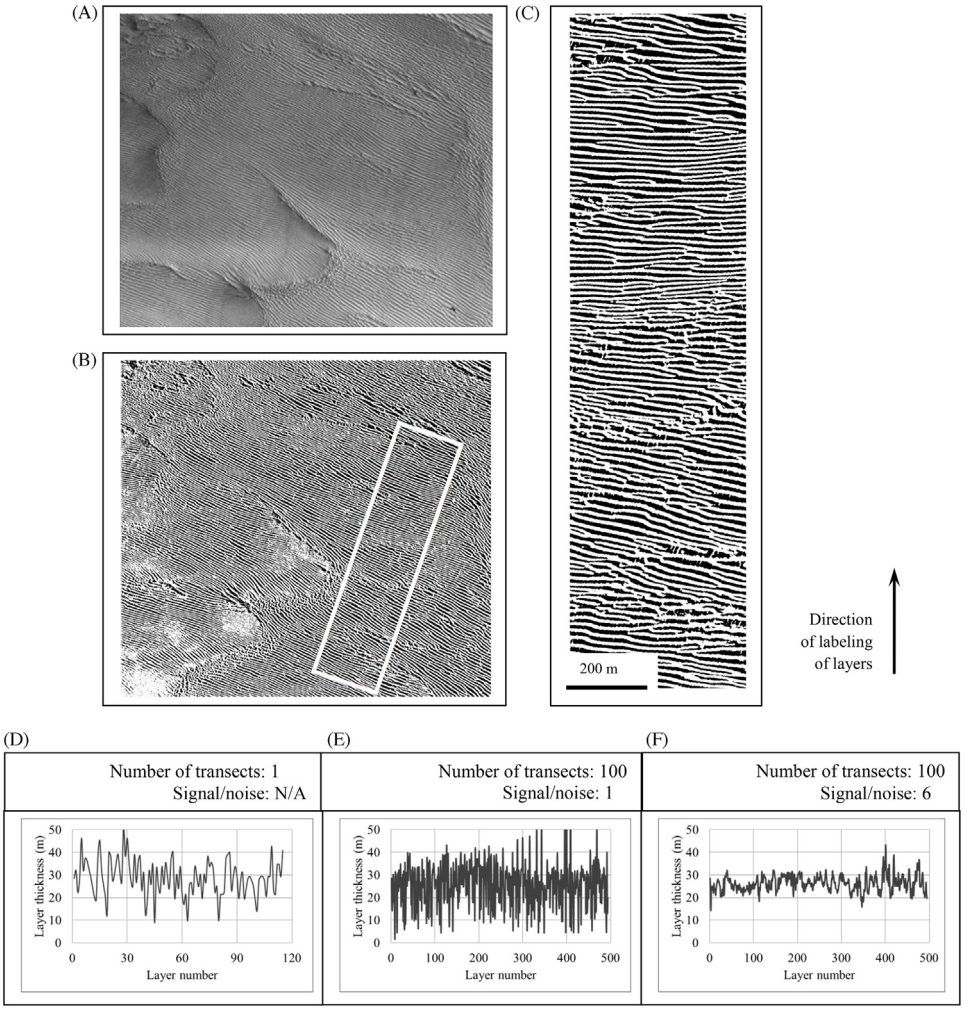

Fig. 11. Variability of layer thickness across Transverse Aeolian Ridges (TAR) on Mars. (A) Grayscale TAR image E03-02283 (Wilson and Zimbelman, 2004). NASA/JPL/Malin Space Science Systems. (B) Black and white TAR image. White rectangle is the sampling area. (C) Sampling area of TAR image. (D) Variability of layer thickness along an arbitrarily chosen transect. (E) Variability of layer thickness across 100 transects for one version, V_1, of layer structure. The distance between transect R_j and R_{j+1}, $j = 1{,}100$ is ~5.3 meters. (F) Variability of layer thickness across 100 transects averaged over versions $V_1, \ldots, V_{36}$ of layer structure.

Three charts for "layer thickness vs. layer number" are plotted for the sampling area (Fig. 11C). The first chart represents the variability of layer thickness along an arbitrarily chosen transect (Fig. 11D). The notion of a signal-to-noise ratio is not applicable for this chart, because this transect does not represent a 2-D layered pattern. The second chart represents layer thickness across 100 transects for one arbitrarily chosen version, V_q, of layer structure (Fig. 11E). For this chart, the signal-to-noise ratio equals 1. To increase the signal-to-noise ratio, thirty-six different versions—$V_1, \ldots, V_{36}$—of this layer structure were generated, resulting in chart sequence $TH = f_1(Ln), \ldots, TH = f_q(Ln), \ldots,$

http://dx.doi.org/10.1016/j.heliyon.2016.e00079

TH = f_{36}(Ln). Fig. 6F depicts chart TH = F(Ln) averaged over TH = f_q(Ln), . . . , TH = f_q(Ln), . . . , TH = f_{36}(Ln). For TH = F(Ln), the signal-to-noise ratio is $\sqrt{36} = 6$.

Chart TH = F(Ln) is the source of N charts TH = F_1(Ln), . . . , TH = F_p(Ln), . . . , TH = F_N(Ln), shown in Fig. 12A, which describe the layer thickness variability across N transects with different levels of detail. Chart #1 (TH = F_1(Ln); Fig. 12B) takes into account all layers regardless of length—even the shortest layers crossing only one transect—meaning that it describes layer thickness variability across N transects with the highest level of confidence. These short layers could be interpreted as noise and therefore be excluded from consideration. Chart #2 is Chart #1 minus layers with PL(A_i) = 1 (Fig. 12B), and Chart #3 is Chart #2 minus layers with PL(A_i) = 2. Chart #N only includes layers crossed by N transects. Each chart from the sequence Chart #1, . . . , Chart #p, . . . , Chart #N is accompanied by the index of confidence, $ICnf_p$ (Fig. 12C).

Fig. 13A and B represent the results of averaging Charts #4–#9 for layer thickness and area across 100 transects. Charts #4–#9 were chosen for averaging because the coefficient of linear correlation between each pair of Charts #4–9 is > 0.81 (thus all of these charts have similar shapes) and the index of confidence for these charts is very high, > 0.96 (Fig. 12C), meaning that Charts #4–#9 are robust for layer size variability across the sampling area of the 2-D layered landform.

3.2. Rub' al Khali dunes: signal-to-noise ratios and chart fuzziness

The Digital Elevation Model (Amante and Eakins, 2009), available via the Discovery Portal of the National Center for Environmental Information of NOAA (http://ngdc.noaa.gov/mgg/dem/), is the source of the image of linear dunes in the Rub' Al Khali desert (Fig. 14A). The parameters of the procedure for converting the grayscale sampling area (Fig. 14A, rectangle in the white frame) to a binary (Fig. 14B) are as follows (Section 2.3.1):

- Resample; width: 700%; height: 700%.
- Emboss; depth: 20; level: 495; direction: 90.
- Convert image to binary; conversion method: line art; threshold: 83.

Fifty transects are used to quantify the variability of layer thickness across the sampling area. The distance between adjacent transects is 2250 meters. Thirty-six different versions of layer structure (V_1, . . . , V_q, . . . , V_{36}) are constructed. Chart TH = f_q(Ln) is associated with version V_q of layer structure;

http://dx.doi.org/10.1016/j.heliyon.2016.e00079

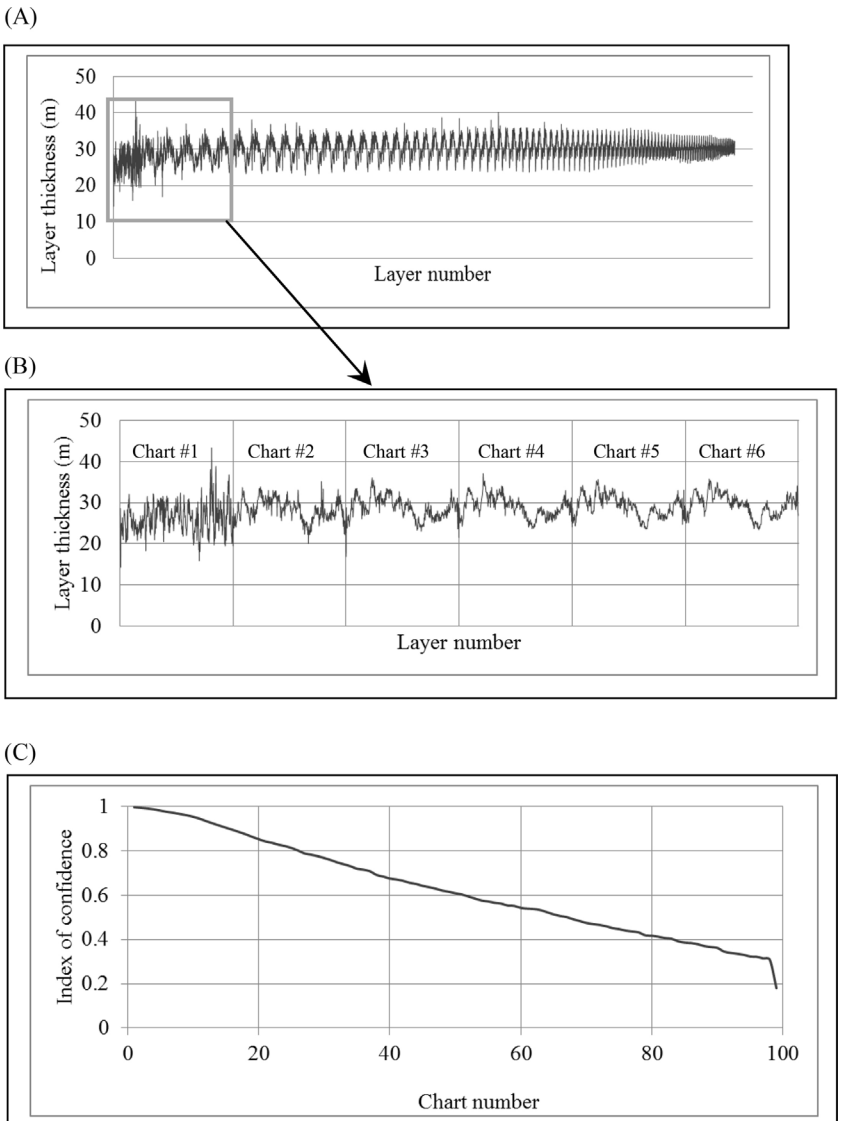

Fig. 12. Opposite tendencies in the construction of TH = F(Ln): level of noise vs. index of confidence. (A) 100 transects create 100 charts TH = F_p(Ln), p = 1, 100. Each chart TH = F_p(Ln) describes layer thickness variability across 100 transects with different level of detail and indices of confidence. (B) Chart #1 takes into account all details of layered landscapes, even layers crossed by only one transect. Chart #1 has highest possible level of index of confidence, but is noisy compared to Charts #2. #3, ... Chart #2 is equal to Chart #1 minus the number of layers crossed by a single transect. Thus, Chart #p = Chart #(p-1) minus number of layers crossed p-1 transects. (C) The plot of "index of confidence vs. chart number" allows a compromise between high signal-to-noise ratios and low indices of confidence (or vice versa). The plot indicates that noise levels for Chart #3 decrease significantly compared to Chart #1, while the index of confidence for Chart #3 ≈ index of confidence for Chart #1.

http://dx.doi.org/10.1016/j.heliyon.2016.e00079

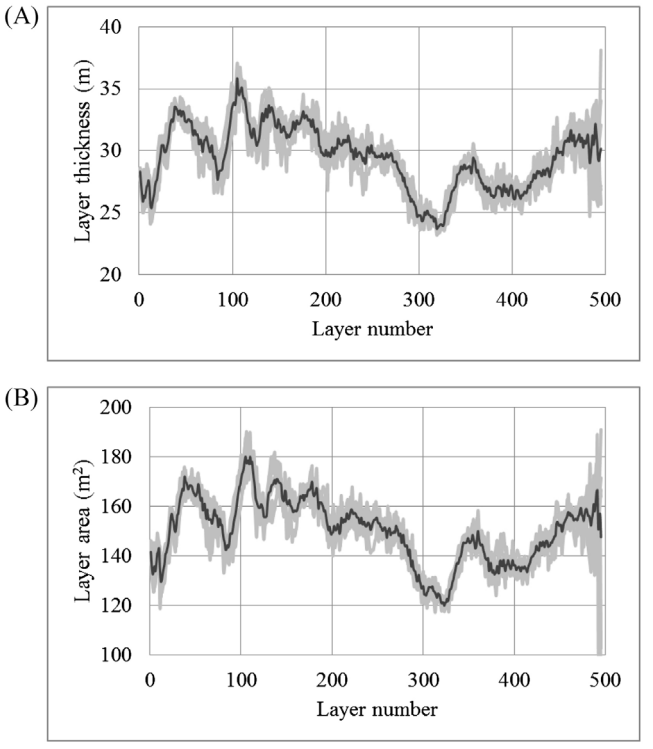

Fig. 13. Layer thickness vs. Layer areas. Number of transects: 100. The distance between transect R_j and R_{j+1}, j = 1,100 is ~5.3 meters. (A) Variability of layer thickness across 100 transects as a result of averaging Charts #4–9. Index of confidence = 0.96. Coefficient of linear correlation between Charts #4–9 ≥ 0.820. (B) Variability of layer areas across 100 transects as a result of averaging Charts #4–9. Index of confidence = 0.96. Coefficient of linear correlation between Charts #4–9 ≥ 0.820.

the signal-to-noise ratio, {TH = f_q(Ln)}, is equal to 1. Charts associated with V_1, . . . , V_{36} are averaged, resulting in TH = F(Ln), which has a signal-to-noise ratio of 6. Charts TH = F_1(Ln), . . . , TH = F_p(Ln), . . . , TH = F_{50}(Ln) are generated by TH = F(Ln) (Fig. 14C). Charts TH = F_4(Ln), . . . , TH = F_{13}(Ln) have low noise levels with respect to TH = F_1(Ln), . . . , TH = F_3(Ln) and high levels of the index of confidence (Fig. 14D). Thus, charts TH = F_4(Ln), . . . , TH = F_{13}(Ln) are averaged (Fig. 14E). The chart shows clear trends in dune thickness variability across the sampling area.

The next experiment evaluates the influence of sampling density on the shape of charts TH = F(Ln) and AR = F(Ln). Fig. 15A and B depict variability of layer thickness and area and the index of confidence across 5 and 150 transects, respectively. A comparison of the charts in Fig. 15A and B makes it clear that even low sampling density (five transects) generates charts with nonchaotic variability of layer thickness and area across the sampling region. Additionally, TH(average 4–13) = F(Ln) generated by fifty transects (Fig. 14E) is

http://dx.doi.org/10.1016/j.heliyon.2016.e00079

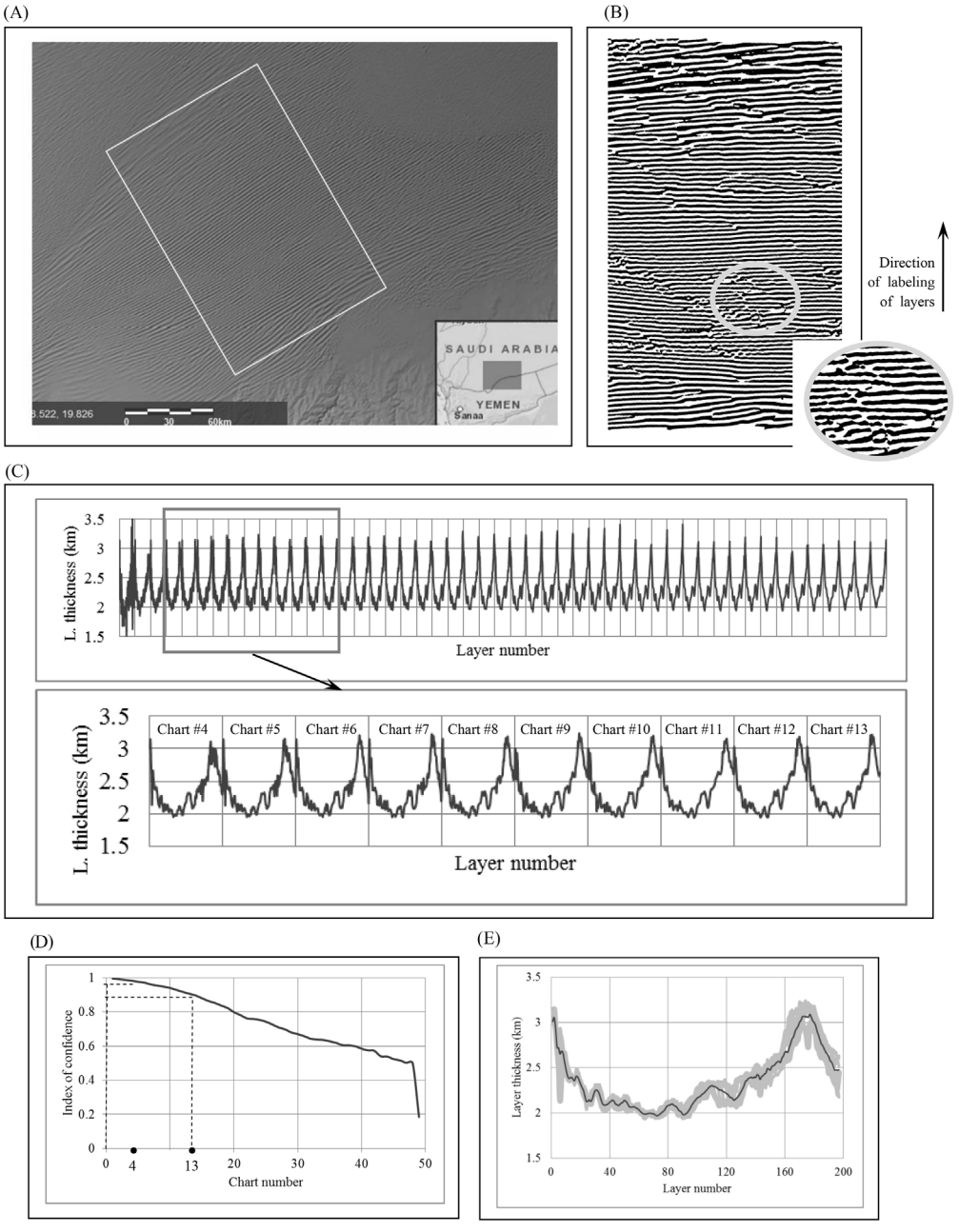

Fig. 14. Variability of dune size across the Rub' al Khali desert. (A) Grayscale pattern of linear dunes in the Rub' al Khali desert. The rectangle in the white frame is the sampling area. (B) The sampling area in black and white. (C) Set of charts generated by TH = F(Ln). Each chart describes layer thickness variability across the sampling area with different levels of noise and indices of confidence. (D) Linear trend in the variability of index of confidence (ICnf) shows slow decrease of ICnf over Charts #4–13, while noise decreases substantially (Fig. 14E). (E) Plot "layer thickness vs. layer number" is the result of averaging Charts #4–13. The average index of confidence for Charts #4-13 is 0.950.

http://dx.doi.org/10.1016/j.heliyon.2016.e00079

indistinguishable from TH(average 3–20) = F(Ln) generated by 150 transects (Fig. 15B). Thus, fifty transects are sufficient to quantify the variability of layer thickness and area in the region of study (Fig. 14B).

The next experiment illustrates the uncertainty of setting correspondence between points on the x-axis of TH = F(Ln) and corresponding layers in a 2-D layered landform. Fig. 16A depicts the variability of layer thickness across fifty transects. The signal-to-noise ratio for the chart in Fig. 16A is 6. Six points on the x-axis of chart TH = F_4(Ln) are labeled with letters A–F (Fig. 16A). Graph G(N) is used to trace the position of A–F in the sampling area of the 2-D landform. Fig. 16B provides evidence that each point on the x-axis of TH = F(Ln) corresponds to more than one layer in the sampling area of the 2-D landform. If the signal-to-noise ratio for TH = F(Ln) is increased, then correspondence between points on the chart (Fig. 16A) and layers in the sampling area become fuzzier.

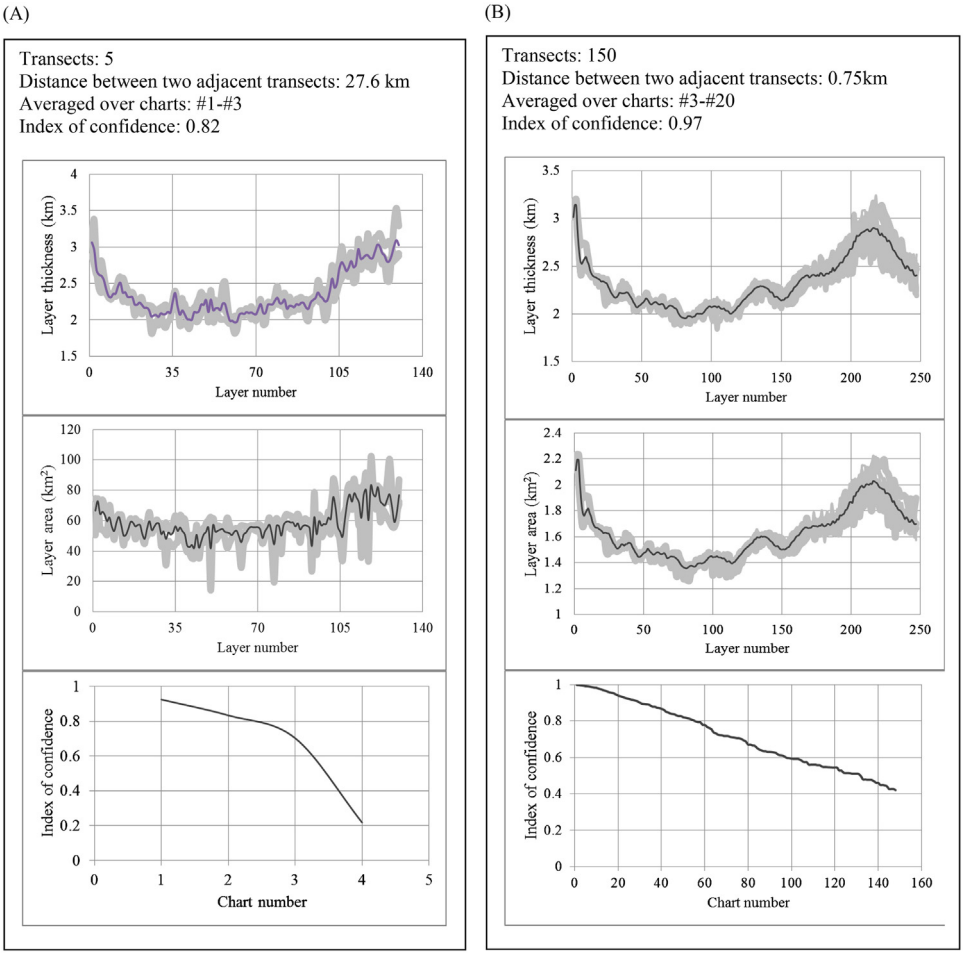

Fig. 15. Robustness of charts TH = F(Ln) and AR = F(Ln) with respect to change in sampling density: 5 transects vs. 150 transects. (A) 5 transects. Distance between two adjacent transects is 27.6 km. (B) 150 transects. Distance between two adjacent transects is 0.75 km.

http://dx.doi.org/10.1016/j.heliyon.2016.e00079

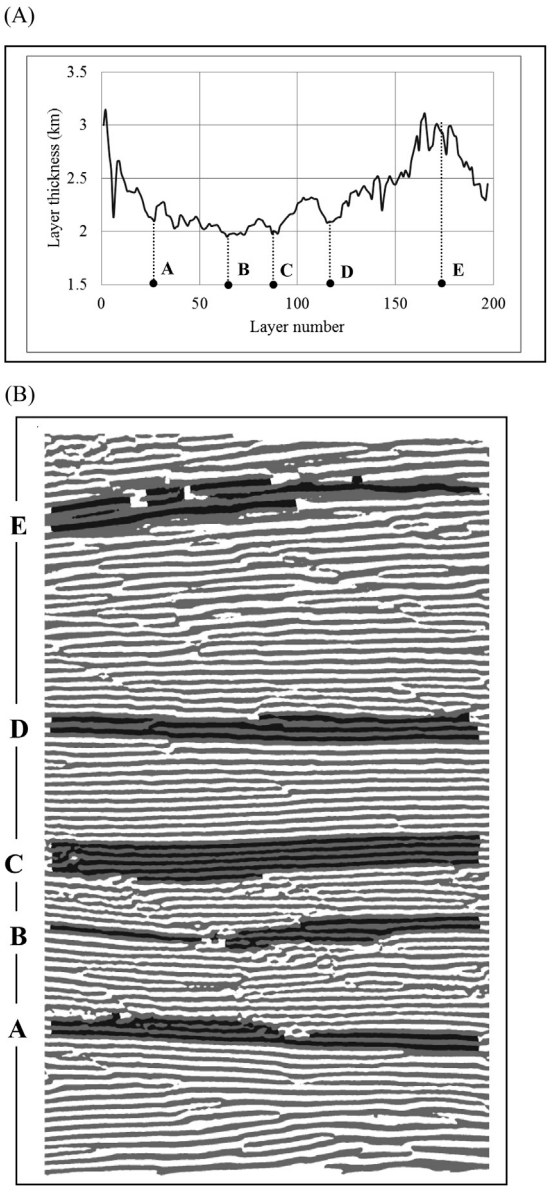

Fig. 16. Points on chart TH = F(Ln) vs. layers in sampling area. (A) Variability of layer thickness across 50 transects for Chart #4. Six points on the x-axis are labeled with letters A–E. The signal-to-noise ratio for Chart #4 is 6. (B) Each point on the x-axis corresponds to more than one layer on the 2-D pattern. If the signal-to-noise ratio for Chart #4 increases, then the correspondence between points on the x-axis and layers in the 2-D pattern becomes fuzzier. Thus, to precisely identify the positions of layers on 2-D patterns and corresponding points on the x-axis of TH = F (Ln) and AR = F(Ln) are mutually exclusive goals.

http://dx.doi.org/10.1016/j.heliyon.2016.e00079

3.3. Transverse Aeolian Ridges on Mars: layer thickness vs. layer area

Fig. 17A depicts grayscale images of Transverse Aeolian Ridges on Mars (Balme et al., 2008). The parameters of the procedure for converting the grayscale image to a binary (Fig. 17B) are as follows (Section 2.3.1):

- Resample; width: 1000%; height: 1000%.
- Emboss; depth: 20; level: 495; direction: 30.
- Convert image to binary; conversion method: line art; threshold: 55.

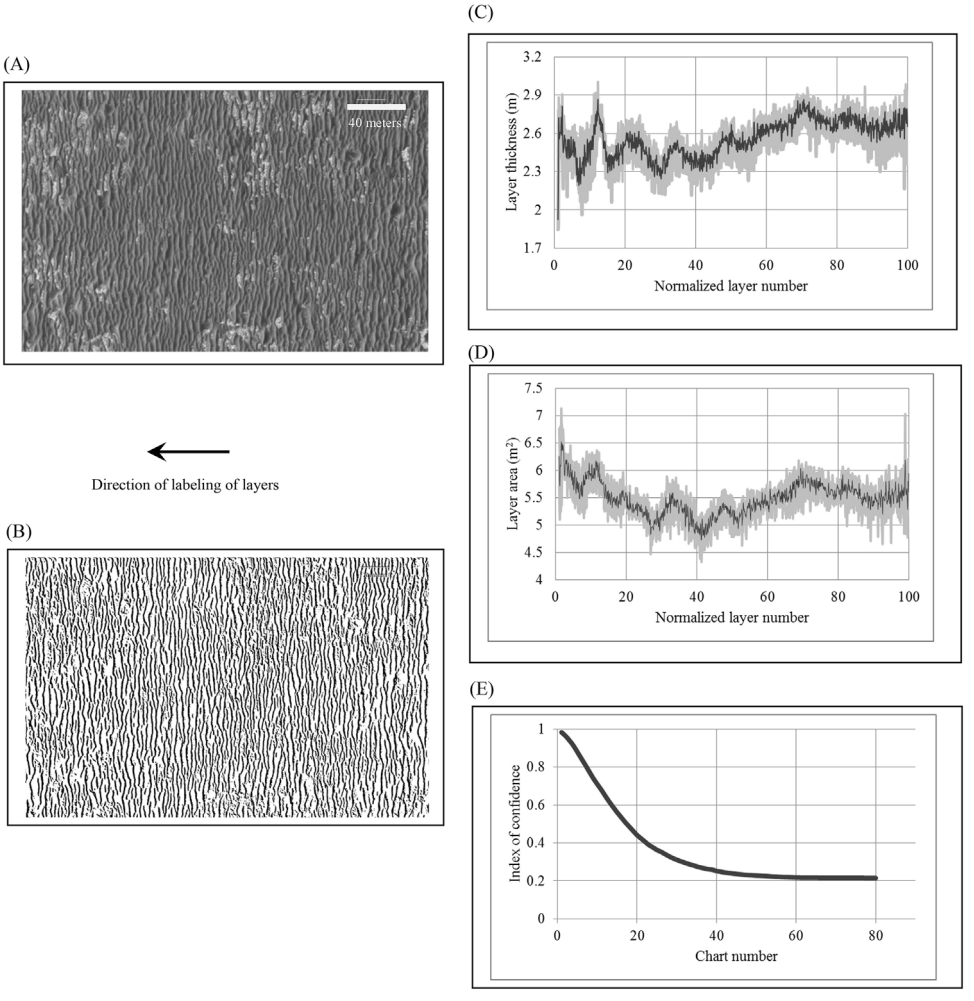

Fig. 17. Transverse Aeolian Ridges (TAR) on Mars: Variability of layer thickness and area across 81 transects of HiRISE image PSP_001414_1780_RED. The distance between transects R_j and R_{j+1}, j = 1,81 is ~2.30 meters. (A) Grayscale sampling area of TAR. (B) Black and white sampling area of TAR. (C) Chart "layer thickness vs. layer number". (D) Chart "layer area vs. layer number. (E) Nonlinear trend in the variability of index of confidence (ICnf) shows significant decrease of ICnf over Charts #1–20: ICnf(Chart #1) = 1, ICnf(Chart #20) = 0.4.

http://dx.doi.org/10.1016/j.heliyon.2016.e00079

Eighty-one transects are used to plot TH = F(Ln) and AR = F(Ln). The distance between two adjacent transects is 2.3 meters. Fig. 17C and D illustrate the variability of layer thickness and area across eighty-one transects.

Compare the plots "index of confidence vs. chart number" for experiments 1 (Fig. 17E) and 3 (Fig. 15B) and denote these charts by ICnf(Exp 1) and ICnf (Exp 3). The chart ICnf(Exp 3) exhibits minor changes over Charts #1–#20, whereas ICnf(Exp 1) exhibits significant changes over Charts #1–#20. For instance, ICnf(Exp 1, Chart #20) > 0.8 (Fig. 15B) and ICnf(Exp 1, Chart #20) = ~0.4 (Fig. 17E). Thus, TH = F(Ln) and AR = F(Ln) in experiment 3 are more robust than those in experiment 1.

3.4. Human bone lamellae

Fig. 18A depicts binary image of human bone lamellae. Seventy-five transects are used to plot TH = F(Ln) (Fig. 18B) and AR = F(Ln) (Fig. 18C). Fig. 18D illustrate the variability of Index of confidence (Eq. (3)).

3.5. Iguana bone lamellae

Fig. 19A depicts grayscale images of iguana bone lamellae. The parameters of the procedure for converting the grayscale image to binary (Fig. 19B) are as follows (Section 2.3.1):

- Resample;width: 1000%; height: 1000%.
- Emboss;depth: 20; level: 495; direction: 30.
- Convert image to binary; conversion method: line art; threshold: 55.

Fifty transects are used to plot TH = F(Ln) (Fig. 19C) and AR = F(Ln) (Fig. 19D). Fig. 19E illustrate the variability of Index of confidence (Eq. (3)).

4. Discussion

4.1. Layered landforms vs. bone lamellae: similarity in processing

Layer characteristics result from the cumulative effects of various internal and external factors that form the size and structure of landforms (Andreotti et al., 2009; Lorenz et al., 2010; Milkovich and Head, 2005) and biological systems (Klevezal, 1996; Bromage et al., 2009). Thus charts TH = f(Ln) and AR = f (Ln) are digital records of states of these factors across the 2-D plane.

Charts TH = f(Ln) and AR = f(Ln) for layered landforms and biological images exhibit similar characteristics: high levels of noise (Fig. 11E), clear trends after

http://dx.doi.org/10.1016/j.heliyon.2016.e00079

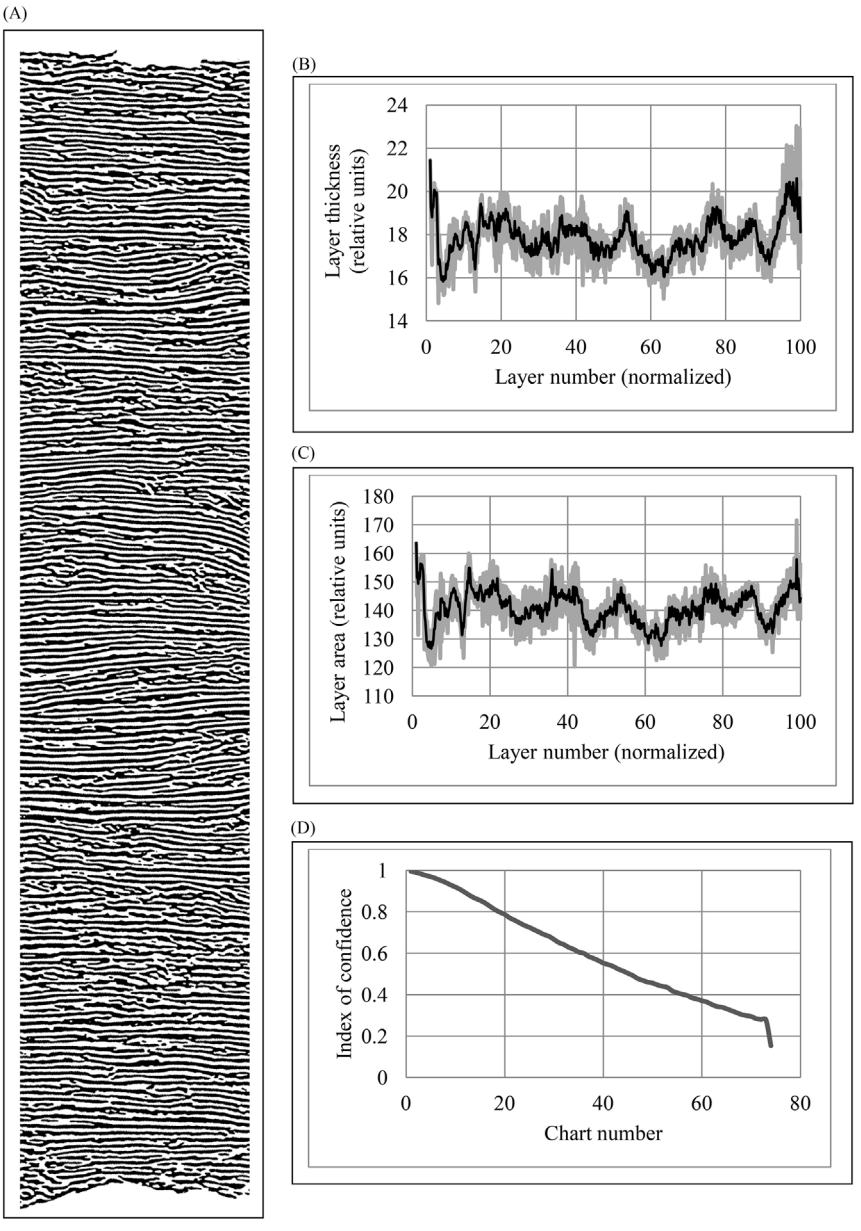

Fig. 18. Lamella bone of a human: Variability of layer thickness and areas across 75 transects. (A) Binary image of lamella bone of human. (B) Chart "layer thickness vs. layer number". (C) Chart "layer area vs. layer number". (D) Chart "index of confidence vs. chart number".

noise reduction (Fig. 13A, B; Fig. 14E; Fig. 15B; Fig. 17C, D; Fig. 18B, C; Fig. 19B, C), and cyclic variability of layer thickness and areas across the 2-D plane (Fig. 15B; Gossel and Laehne, 2013).

From an algorithmic point of view, layered landforms and biological patterns have anisotropic structures, which may be described in terms of an N-partite

http://dx.doi.org/10.1016/j.heliyon.2016.e00079

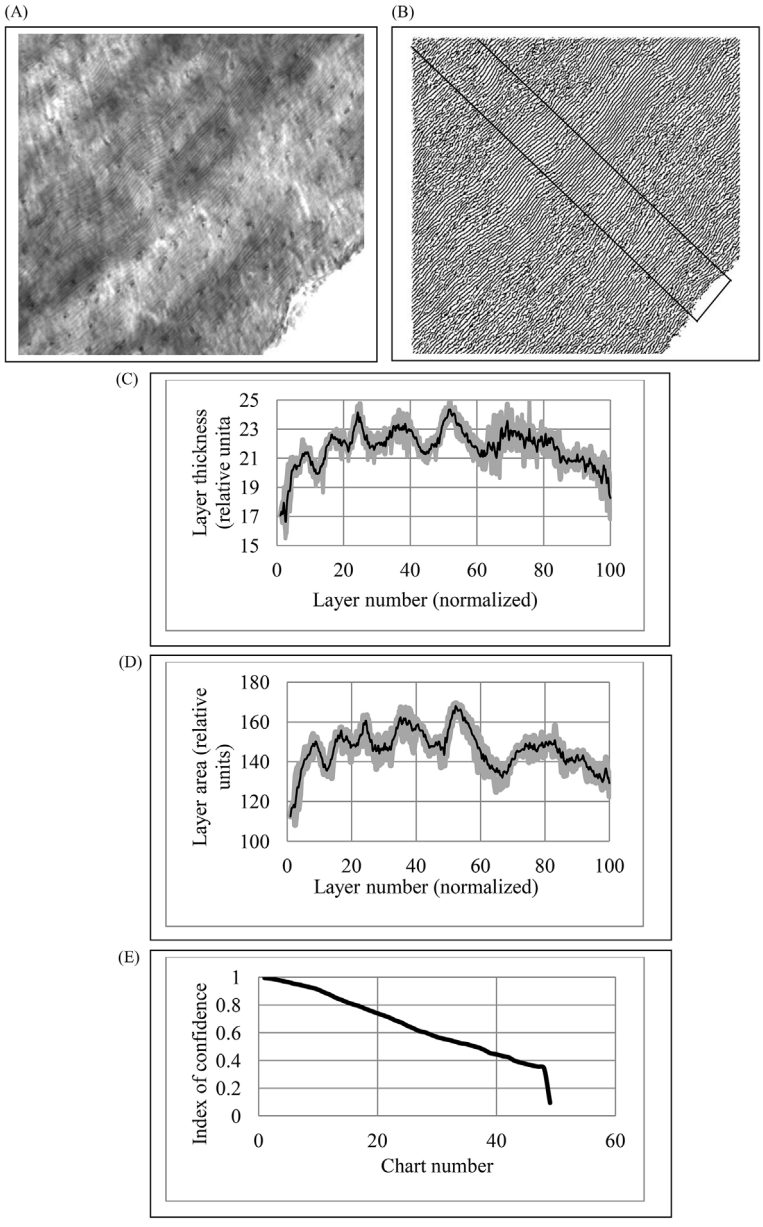

Fig. 19. Lamella bone of a iguana: Variability of layer thickness and areas across 50 transects. (A) Grayscale and (B) binary image of lamella bone of iguana. (C) Chart "layer thickness vs. layer number". (D) Chart "layer area vs. layer number". (E) Chart "index of confidence vs. chart number".

graph and Boolean functions. This similarity permits us to use the same formal procedure for converting layered patterns into a pure mathematical model.

Structural anisotropy of layered patterns leads to uncertainty in determining the correspondence between points on TH = F(Ln) and AR = F(Ln) and in layers on the 2-D pattern; each point corresponds to more than one layer on the 2-D

http://dx.doi.org/10.1016/j.heliyon.2016.e00079

layered pattern, and each layer on the pattern contributes to calculations of the average thickness and area of more than one point on TH = F(Ln) and AR = F (Ln). Thus, to precisely identify the positions of layers on 2-D patterns and corresponding points on the x-axis of TH = F(Ln) and AR = F(Ln) are mutually exclusive goals.

4.2. Layered landforms vs. bone lamellae: differences in interpretation

In the case of biological systems, incremental layers follow each other in time. That is, each layer is a time marker; the sampling area has one layer with marker "time begins" and one layer with marker "time ends." In contrast, it is impossible to identify "time begins" and "time ends" for some categories of layered landforms. For instance, linear (longitudinal) dunes form parallel to a wind vector (Tsoar, 1989). From this it follows that various dunes (layers) are formed at the same instant of time. This statement is also true for some biological systems. For instance, fingerprint ridges form simultaneously in different regions (Kücken and Newell, 2005).

Consider the procedure for constructing TH = f(Ln) and AR = f(Ln) from the standpoint of synchronizing layer formation in the space-time domain. Transects R_j and R_{j+1} are represented by time scales T_j and T_{j+1}. Let us assume that layer $\mathbf{P}_{i,j}$ was formed at time $t_{i,j}$. Additionally, layer $\mathbf{P}_{i,j}$ could correspond to more than one layer crossed by transect R_{i+1} due to the anisotropic structure of the 2-D layered landform. Thus, it is necessary to define the structure of layer $\mathbf{P}_{i,j}$ across the 2-D plane in order to calculate the variability of the layer's thickness and area across transects R_j and R_{j+1}.

The process of connecting the vertices situated on R_j with vertices situated on R_{j+1} (Fig. 2A) is a process of synchronizing layer formation in time scales T_j and T_{j+1}, or more precisely in spatial-temporal scales T_j and T_{j+1}. This is due the fact that transect R_j as well as corresponding scale T_j represents characteristics of layered patterns in the space-time domain.

Graphs and Boolean functions are the quantitative description of all possible versions of the synchronization of layers formed across a 2-D plane over a period of time. Thus, charts TH = f(Ln) and AR = f(Ln) represent the set of repeating observations of average layer thickness and area across the 2-D plane. Because the average thickness/area of layer $\mathbf{P}_i$ is the measure of the average formation rate of layered biological systems at an instant of time T_i across a 2-D plane, TH = f(Ln) and AR = f(Ln) represent the growth-rate variability of a 2-D layered biological system in the space-time domain.

http://dx.doi.org/10.1016/j.heliyon.2016.e00079

Graph and Boolean function are tools only for the synchronization of layered formation in the spatial domain of 2-D layered landforms only (because the order of layers in the time domain is unknown). This fact permits us to consider TH = f(Ln) and AR = f(Ln) as spatial series for a 2-D layered landforms.

Consider potential sources of cyclic trends in TH = f(Ln) and AR = f(Ln) for biological layered systems. Two facts about layer formation in biological systems provide the basis for interpretations of the cyclicity of TH = f(Ln) and AR = f(Ln). The first fact is that the thickness of layers is proportional to the growth rate of an incremental system. The second fact is that layers follow each other in time.

Cyclicity in human bone has only just begun to be documented. Evidence to date has revealed a six- to eight-week rhythm as well as the occasional observance of an annual rhythm (Bromage et al., 2011). Annual rhythms are known to occur in seasonal environments that experience yearly oscillations in resource availability (Klevezal, 1996). In humans, annual cyclicity may be explained by resource availability for individuals living under natural circumstances. However, a six- to eight-week rhythm does not align with any known endogenous physiological or exogenous environmental rhythm. Because we can approximate the number of lamellae, and thus time, along the layer number axis, we estimate that the lamellae formed over approximately 194 weeks (Fig. 18), from which we know that each lamella represents about eight days of bone formation (Bromage et al., 2011). Fig. 18B is a chart of layer thickness vs. layer number, wherein the bone growth-rate variability structure reveals high-frequency variability on the order of two weeks, while lower frequency variability is also present. Even lower frequency oscillations exist in the time domain of six months, plus or minus. These results are interesting because we observe that the developed method allows us discover rhythms that do not have an immediate environmental or physiological explanation.

Cyclicity in iguana bones is caused by external environmental factors, presumably largely temporal differences in food supply and temperature. These key environmental features vary on time scales of a day to weeks and months over an annual cycle. Primarily, for these herbivorous lizards, the production of fresh greenery is important as food input. In their natural habitats in the dry and wet tropics, the seasonality of rainy and dry seasons strongly influence the availability of their preferred plant food. In addition to food intake, digestion plays a major role in how much energy is available to individual organisms for growth, including bone production. The speed of digestion follows a Q10 of ca. 2.5, indicating that at ambient temperature differences of 10 degrees Celsius, digestion differs by a factor of 2.5 fold. Thus, during hot seasons the speed of digestion and associated growth is rapid, while during cold (or wet and cloudy)

http://dx.doi.org/10.1016/j.heliyon.2016.e00079

seasons growth slows dramatically. Similar principles apply to daily changes in temperature and associated speed of digestion and magnitude of energy metabolism (i.e., energy turnover is significantly reduced at night). Taken together, these temporal (daily, seasonal, annual) variations in environmental parameters may be reflected in the layered patterns in iguana bones.

Fig. 19 is an examination of the 2-D layered pattern of femoral bone from a six-month-old laboratory-reared iguana. Laboratory temperature was kept constant, and lighting was controlled to twelve hours on and twelve hours off. During the period of bone formation, the animal was given two vital labels (calcein green) twenty-eight days apart. These were incorporated into the mineralizing surface of new bone. From this experiment we were able to conclude that the iguana formed one lamella per day.

Fig. 19B is a chart of layer thickness vs. layer number for which roughly one week is represented for every five units on the layer number scale. First we notice that for each of the first two 20 units on the layer number scale (roughly 0–40), there are two pronounced increases in growth rate. This is followed by one large increase lasting between roughly 45–65. Given that environmental conditions remained constant, the two-weekly growth rate variability is a rhythm without any known biological foundation, but it must be fundamental. This rhythm became accentuated during roughly 45–65 and again between roughly 65–85 units on the layer number scale, but there is no biological or environmental explanation at present.

Finally we would like to point out that the possibility also exists that using the developed method we can discover rhythms that do not have an immediate environmental, geological, or physiological explanation.

4.3. Noise reduction

Three levels of noise reduction are used to improve the signal-to-noise ratio in TH = f(Ln) and AR = f(Ln). First, binary segments of the layered pattern not associated with layers are removed from the image (Section 2.3.4). Second, thirty-six versions of the layer structure (V_1, . . . , V_q, . . . , V_{36}) are generated; chart TH = f_q(Ln) is plotted for each version, V_q. The signal-to-noise ratio for TH = f_q(Ln) is equal to 1. Charts TH = f_1(Ln), . . . , TH = f_{36}(Ln) are averaged, resulting in TH = F(Ln). The signal-to-noise ratio for TH = F(Ln) is equal to $\sqrt{36} = 6$ (Section 2.2.3). Thirty-six versions of layer structure were arbitrarily chosen to illustrate the possibility of substantially reducing noise in charts TH = f(Ln) and AR = f(Ln).

Chart TH = F(Ln) takes into account 99% of the sampling area; in other words, the index of confidence for TH = F(Ln) is 0.99 (Fig. 12C) because TH = F(Ln) takes

http://dx.doi.org/10.1016/j.heliyon.2016.e00079

into account all layers regardless of their lengths. The third level of noise reduction is based on the assumption that the greater the length, PL($\mathbf{P}_i$), of layer $\mathbf{P}_i$, the more that layer has been sampled by transects. Therefore, there is a higher certainty that the average thickness of $\mathbf{P}_i$ is a measure of real characteristics of the 2-D layered pattern rather than a source of noise. A smaller value of PL($\mathbf{P}_i$) reflects more anisotropy and therefore less certainty about the variability of the thickness of layer $\mathbf{P}_i$ across the 2-D plane.

The index of confidence allows a compromise between more detail and a lower signal-to-noise ratio or less detail and a higher signal-to-noise ratio in describing the variability of layer thickness across N transects. It is therefore possible to plot the most robust charts TH = F(Ln) and AR = F(Ln).

4.4. Assumptions

Assumption #1. Factors controlling layer formation within the sampling area are constant. If this assumption is valid, then the identical procedure of scale linkage is applicable to all layers within the sampling area.

Assumption #2. Layer size is unimodally distributed across N transects. This assumption permits the average size of layers to be calculated. If this assumption is not valid (e.g., layer thicknesses are distributed bimodally), then the idea of an average layer size across the sampling area makes no sense. If this assumption fails, then a new problem arises, such as finding the subarea of maximal size with unimodal characteristics within a sampling area that has bimodally distributed layer size.

4.5. Limitations

- Limitation #1. The proposed method is not applicable to formalizing the size and structure of three-dimensional layered objects.
- Limitation #2. Transects must be perpendicular or quasiperpendicular to layers in order to avoid errors in calculating layer thickness. The parameter for “layer area” is not sensitive to the angle at which a transect crosses the layer.
- Limitation #3. Transects must be straight lines.
- Limitation #4. The distance between each pair of transects R_j and R_{j+1} must be constant across the sampling area.

With respect to Limitation #1, technologies such as Ground Penetrating Radar (landforms) and serial sectioning (incremental patterns) make it possible to trace layered structures in 3-D space. Models of 2-D layered patterns with anisotropy must be modified in order to be applicable for the quantification of 3-D layered

http://dx.doi.org/10.1016/j.heliyon.2016.e00079

patterns. Limitations #2–5 result from technical limits of current software. It is possible that these limitations will be overcome in the future.

4.6. Areas of application

Layered patterns are broadly distributed in nature (Ball, 1999; Rubin, 2006), and new nanotechnologies are also a source of self-assembled ripple patterns with anisotropy (Lian et al., 2006; Peng et al., 2008) similar to layered biological and geological patterns. Additionally, Discrete Elevation Model data (Amante and Eakins, 2009), hundreds of thousands of satellite images of the surface of Earth and other planets (Bourke et al., 2010; Neish et al., 2010; McEwen et al., 2007), and an abundant supply of incremental biological patterns are available for study but require various automated procedures before they can be readily analyzed. The proposed method is applicable to plot special-time and spatial series for layered systems of different origins.

The empiric model of layered patterns with structural anisotropy could be used for solving various problems relating to the study of layered systems and formation mechanisms. For instance, an N-partite graph G(N) could be used to reveal the evolution of a layered aeolian system over time. Charts TH = F(Ln) and AR = F(Ln) could measure the adequacy of a model of 2-D layered pattern formation.

Boolean functions (i.e., the idea of gates being open or closed) can provide tools to quantify the sensitivity of charts TH = F(Ln) and AR = F(Ln) to the variability of 2-D layered landform structure. In addition, the distribution of values of the index of structural anisotropy across a 2-D plane could also be a source of information about the history of pattern formation (Smolyar and Bromage, 2004).

5. Conclusion

The output of the developed method (i.e., charts TH = F(Ln) and AR = F(Ln)) form the basis for applying the quantitative method of analyzing the variability of layer thickness across a 2-D plane, with an aim to reconstruct events in the history of the layered systems formation. Graphs and Boolean functions, which allow the structure of layered systems to be quantified, are key tools for formalizing 2-D layered patterns. From a mathematical perspective, 2-D layered objects have some of the simplest geometrical structures found in nature, which is why graphs and Boolean functions are sufficient to adequately describe 2-D layered patterns with anisotropic size and structure. These mathematical tools provide numerous possibilities for formalizing layered-pattern analysis.

http://dx.doi.org/10.1016/j.heliyon.2016.e00079

Declarations

Author contribution statement

Igor Smolyar, Timothy Bromage, Martin Wikelski: Conceived and designed the experiments; Performed the experiments; Analyzed and interpreted the data; Contributed reagents, materials, analysis tools or data; Wrote the paper.

Funding statement

The authors received no funding from an external source.

Competing interest statement

The authors declare no conflict of interest.

Additional information

No additional information is available for this paper.

Acknowledgements

The authors wish to thank Amy Bekkerman of Precision Edits for assistance in editing and formatting the text. Thanks to Galina Vovna for contributing to knowledge of layered landforms. Comments from two anonymous reviewers allowed us to improve the paper. The authors acknowledge the use of Mars Orbiter Camera images processed by Malin Space Science Systems, available at http://www.msss.com/moc_gallery. The views and opinions expressed in this article are those of I. Smolyar and do not necessarily reflect the official policy or position of NOAA.

References

Amante, C., Eakins, B.W., 2009. ETOPO1 1 arc-minute global relief model procedures data sources and analysisNOAA Technical Memorandum NESDIS No. NGDC-24) Boulder CO: National Ocean and Atmospheric Administration 19. Retrieved from http://purl.access.gpo.gov/GPO/gpo441.

Anderson, J.A., 2001. Discrete Mathematics with Combinatorics. Prentice Hall, Upper Saddle River, NJ.

Andreotti, B., Claudin, P., Fourriere, A., Murray, B., Ould-Kaddour, F., 2009. Giant aeolian dune size determined by the average depth of the atmospheric boundary layer. Nature 457 (7233), 1120–1123.

Ball, P., 1999. Nature's patterns: a tapestry in three parts. Oxford University Press, Oxford; New York.

http://dx.doi.org/10.1016/j.heliyon.2016.e00079

Balme, M., Berman, D.C., Bourke, M.C., Zimbelman, J.R., 2008. Transverse Aeolian Ridges (TARs) on Mars. Geomorphology 101 (4), 703–720.

Blumberg, D.G., 2006. Analysis of large aeolian (wind-blown) bedforms using the Shuttle Radar Topography Mission (SRTM) digital elevation data. Remote Sens. Environ. 100 (2), 179–189.

Bourke, M.C., Edgett, K.S., Cantor, B.A., 2008. Recent aeolian dune change on Mars. Geomorphology 94 (1–2), 247–255.

Bourke, M.C., Lancaster, N., Fenton, L.K., Parteli, E.J.R., Zimbelman, J.R., Radebaugh, J., 2010. Extraterrestrial dunes: An introduction to the special issue on planetary dune systems. Geomorphology 121 (1-2), 1–14.

Bromage, T.G., Juwayeyi, Y.M., Smolyar, I., Hu, B., Gomez, S., Chisi, J., 2011. Enamel-Calibrated Lamellar Bone Reveals Long Period Growth Rate Variability in Humans. Cells Tissues Organs 194, 124–130.

Bromage, T.G., Lacruz, R.S., Hogg, R., Goldman, H.M., McFarlin, S.C., Warshaw, J., Dirks, W., Perez-Ochoa, A., Smolyar, I., Enlow, D.H., Boyde, A., 2009. Lamellar bone is an incremental tissue reconciling enamel rhythms, body size, and organismal life history. Calcified Tissue Int. 84 (5), 388–404.

Casselman, J.M., 1983. Age and growth assessment of fish from their calcified structures e techniques and tools. In: Prince, E.D., Pulos, L.M. (Eds.), Proceedings of the International Workshop on Age Determination of Oceanic Pelagic Fishes: Tunas, Billfishes, and Sharks, Miami, Florida, February 15-18, 1982. NOAA/National Marine Fisheries Service, Miami, FL, pp. 1–17.

Ewing, R.C., Peyret, A.-P.B., Kocurek, G., Bourke, M., 2010. Dune field pattern formation and recent transporting winds in the Olympia Undae Dune Field: north polar region of Mars. J. Geophys. Res. Planets 115 (E8), 1–25.

Fenton, L.K., Hayward, R.K., 2010. Southern high latitude dune fields on Mars: Morphology, aeolian inactivity, and climate change. Geomorphology 121 (1–2), 98–121.

Fishbaugh, K.E., Byrne, S., Herkenhoff, K.E., Kirk, R.L., Fortezzo, C., Russell, P.S., McEwen, A., 2010. Evaluating the meaning of layer in the martian north polar layered deposits and the impact on the climate connection. Icarus 205 (1), 269–282.

Fitzsimmons, K.E., 2007. Morphological variability in the linear dunefields of the Strzelecki and Tirari Deserts, Australia. Geomorphology 91 (1-2), 146–160.

 http://dx.doi.org/10.1016/j.heliyon.2016.e00079

Gossel, W., Laehne, R., 2013. Applications of time series analysis in geosciences: An overview of methods and sample applications. Hydrol. Earth Syst. Sci. Discuss. 10, 12793–12827.

Huss, D., 2001. Corel Photo-paint 10: the official guide. Osborne/McGraw-Hill, New York.

Klevezal, G.A., 1996. Recording structures of mammals: determination of age and reconstruction of life history. A.A. Balkema, Rotterdam.

Kücken, M., Newell, A.C., 2005. Fingerprint formation. J. Theor. Biol. 235 (1), 71–83.

Le Gall, A., Hayes, A.G., Ewing, R., Janssen, M.A., Radebaugh, J., Savage, C., Encrenaz, P., 2012. Latitudinal and altitudinal controls of Titan's dune field morphometry. Icarus 217 (1), 231–242.

Lian, J., Zhou, W., Wei, Q.M., Wang, L.M., Boatner, L.A., Ewing, R.C., 2006. Simultaneous formation of surface ripples and metallic nanodots induced by phase decomposition and focused ion beam patterning. Appl. Phys. Lett. 88 (9), 93112.

Lorenz, R.D., Claudin, P., Andreotti, B., Radebaugh, J., Tokano, T., 2010. A 3 km atmospheric boundary layer on Titan indicated by dune spacing and Huygens data. Icarus 205 (2), 719–721.

McEwen, A.S., Eliason, E.M., Bergstrom, J.W., Bridges, N.T., Hansen, C.J., Delamere, W.A., Grant, J.A., Gulick, V.C., Herkenhoff, K.E., Keszthelyi, L., Kirk, R.L., Mellon, M.T., Squyres, S.W., Thomas, N., Weitz, C.M., 2007. Mars Reconnaissance Orbiter's High Resolution Imaging Science Experiment (HiRISE). J. Geophys. Res. Planets 112 (E5), 1–40.

Milkovich, S.M., Head III, J.W., 2005. North polar cap of Mars: Polar layered deposit characterization and identification of a fundamental climate signal. J. Geophys. Res. Planets 110 (E1), 1–21.

Montgomery, D.R., Bandfield, J.L., Becker, S.K., 2012. Periodic bedrock ridges on Mars. J. Geophys. Res. Planets 117 (E3), 1–12.

Nature Methods, 2012. The quest for quantitative microscopy. Nature Methods: Editorial627.

Neish, C.D., Lorenz, R.D., Kirk, R.L., Wye, L.C., 2010. Radarclinometry of the sand seas of Africa's Namibia and Saturn's moon Titan. Icarus 208 (1), 385–394.

Peng, H., Xie, C., Schoen, D.T., Cui, Y., 2008. Large anisotropy of electrical properties in layer-structured In2Se3 nanowires. Nano Letters 8 (5), 1511–1516.

 http://dx.doi.org/10.1016/j.heliyon.2016.e00079

Roberts, F.S., 1976. Discrete mathematical models, with applications to social, biological, and environmental problems. Prentice-Hall, Englewood Cliffs, N.J.

Rosenfeld, A., Kak, A.C., 1982. Digital picture processing. Academic Press, New York.

Rubin, D.M., 2006. Ripple effect: Unforeseen applications of sand studies. Eos 87 (30), 293–297.

Rubin, D.M., Tsoar, H., Blumberg, D.G., 2008. A second look at western Sinai seif dunes and their lateral migration. Geomorphology 93 (3–4), 335–342.

Smolyar, I.V., 2014. System and method for quantification of size and anisotropic structure of layered patterns. U.S. Patent 8,755,578, issued June 17, 2014.

Smolyar, I.V., Bromage, T.G., 2004. Discrete model of fish scale incremental pattern: a formalization of the 2D anisotropic structure. ICES J. Mar. Sci. 61 (6), 992–1003.

Thomas, D.S.G., Knight, M., Wiggs, G.F.S., 2005. Remobilization of southern African desert dune systems by twenty-first century global warming. Nature 435 (7046), 1218–1221.

Tsoar, H., 1989. Linear dunes – forms and formation. Prog. Phys. Geog. 13 (4), 507–528.

Tsoar, H., 2005. Sand dunes mobility and stability in relation to climate. Physica A 357 (1), 50–56.

van Drongelen, W., 2007. Signal processing for neuroscientists: introduction to the analysis of physiological signals. Academic Press, Burlington, Mass.

Wilson, S.A., Zimbelman, J.R., 2004. Latitude-dependent nature and physical characteristics of Transverse Aeolian Ridges on Mars. J. Geophys. Res. Planets 109 (E10), 1–12.

Zimbelman, J.R., 2010. Transverse Aeolian Ridges on Mars: First results from HiRISE images. Geomorphology 121 (1–2), 22–29.

Yizhaq, H., Isenberg, O., Wenkart, R., Tsoar, H., Karnieli, A., 2009. Morphology and dynamics of aeolian mega-ripples in Nahal Kasuy southern Israel. Isr. J. Earth Sci. 57, 149–165.

 http://dx.doi.org/10.1016/j.heliyon.2016.e00079